THE JOURNAL OF BIOLOGICAL CHEMISTRY VOL. 291, NO. 18, pp. 9396–9410, April 29, 2016
Published in the U.S.A.

RNF8 E3 Ubiquitin Ligase Stimulates Ubc13 E2 Conjugating Activity That Is Essential for DNA Double Strand Break Signaling and BRCA1 Tumor Suppressor Recruitment*

Received for publication, January 19, 2016, and in revised form, February 12, 2016 Published, JBC Papers in Press, February 22, 2016, DOI 10.1074/jbc.M116.715698

Curtis D. Hodge[‡], Ismail H. Ismail[§¶1], Ross A. Edwards[‡1], Greg L. Hura[‖], Andrew T. Xiao[‡], John A. Tainer[‖2], Michael J. Hendzel[§], and J. N. Mark Glover[‡3]**

*From the [‡]Department of Biochemistry, University of Alberta, Edmonton, Alberta T6G 2H7, Canada, the [§]Department of Oncology, University of Alberta, Edmonton, Alberta T6G 1Z2, Canada, the [‖]Lawrence Berkeley National Laboratory, Berkeley, California 94704, the **Department of Molecular and Cellular Oncology, University of Texas M.D. Anderson Cancer Center, Houston, Texas 77030, and the [¶]Biophysics Department, Faculty of Science, Cairo University, 12613 Giza, Egypt*

DNA double strand break (DSB) responses depend on the sequential actions of the E3 ubiquitin ligases RNF8 and RNF168 plus E2 ubiquitin-conjugating enzyme Ubc13 to specifically generate histone Lys-63-linked ubiquitin chains in DSB signaling. Here, we defined the activated RNF8-Ubc13~ubiquitin complex by x-ray crystallography and its functional solution conformations by x-ray scattering, as tested by separation-of-function mutations imaged in cells by immunofluorescence. The collective results show that the RING E3 RNF8 targets E2 Ubc13 to DSB sites and plays a critical role in damage signaling by stimulating polyubiquitination through modulating conformations of ubiquitin covalently linked to the Ubc13 active site. Structure-guided separation-of-function mutations show that the RNF8 E2 stimulating activity is essential for DSB signaling in mammalian cells and is necessary for downstream recruitment of 53BP1 and BRCA1. Chromatin-targeted RNF168 rescues 53BP1 recruitment involved in non-homologous end joining but not BRCA1 recruitment for homologous recombination. These findings suggest an allosteric approach to targeting the ubiquitin-docking cleft at the E2-E3 interface for possible interventions in cancer and chronic inflammation, and moreover, they establish an independent RNF8 role in BRCA1 recruitment.

Protein ubiquitination provides a major method of intracellular communication whereby a target molecule is tagged with ubiquitin or ubiquitin chains to confer a specific signal (1). Specifically, an E1-activating enzyme uses ATP to initiate ubiquitin chain synthesis by the formation of a covalent linkage to the C-terminal glycine of ubiquitin (2, 3). The ubiquitin molecule is subsequently transferred to the active site cysteine of an E2-conjugating enzyme, via a trans-thioesterification reaction (3, 4). One of many possible E3 ligases binds both the E2~Ub[4] complex and substrate (RING E3s) or acts as an intermediate to the substrate through the use of an active site cysteine (HECT and RBR E3s) (5, 6).

An important RING E3 ligase for the DNA damage response is RNF8, which binds and activates the E2, Ubc13, to create Lys-63-linked ubiquitin chains (7–13). These chains act as scaffolds for proteins that contain ubiquitin-interacting motifs, such as RAP80, or motifs interacting with ubiquitin (MIUs), such as the RING E3 ligase RNF168, which directly bind ubiquitin (14–17). Both RING E3 ligases RNF8 and RNF168 are recruited to the sites of double strand break (DSB) DNA damage. Initially, broken DNA ends are recognized by the Mre11-Rad50-Nbs1 (MRN) complex that subsequently recruits and activates ATM, which phosphorylates H2AX (γH2AX) within chromatin surrounding the lesion (18, 19). The scaffolding protein MDC1 binds γH2AX through its BRCT domain and is also phosphorylated by ATM (20–22). This allows association of RNF8 to MDC1 through its N-terminal forkhead-associated (FHA) domain (11, 12). RNF8-Ubc13 may then poly-Lys-63 ubiquitinate H1-type linker histones (23), which recruit RNF168 through their MIUs to amplify the signal and monoubiquitinate histones H2A/H2AX on Lys-13/15 (8, 17, 24). RNF8 and RNF168 then cooperate to extend these Lys-63 polyubiquitin chains promoting recruitment of RAP80, BRCA1, and 53BP1, resulting in DSB repair (25, 26). RNF8 and RNF168 are both recruitment factors for Ubc13; however, work with these purified E3 RING domains and Ubc13 have shown that

* This work was supported in part by Canadian Cancer Society/Canadian Breast Cancer Research Alliance (to J. N. M. G.), Canadian Institutes of Health Research Grants CIHR114975 (to J. N. M. G.) and CIHR119515 (to M. J. H.), National Institutes of Health Grant CA92584 (to J. N. M. G. and J. A. T.), and the Alberta Innovates Health Solutions. The authors declare that they have no conflicts of interest with the contents of this article. The content is solely the responsibility of the authors and does not necessarily represent the official views of the National Institutes of Health.

We dedicate this study in memory of Stephen J. Campbell whose hard work and affable personality made a difference.

The atomic coordinates and structure factors (code 4WHV) have been deposited in the Protein Data Bank (http://wwpdb.org/).

SAXS curves have been deposited to Small Angle Scattering Biological Data Bank (http://www.sasbdb.org/) with the codes: WT RNF8-Ubc13~Ub: SASDBR3, L451D RNF8-Ubc13~Ub: SASDBT3, WT RNF8-Ubc13~Ub/Mms2: SASDBS3, L451D RNF8-Ubc13~Ub/Mms2: SASDBU3.

[1] Both authors contributed equally to this work.

[2] Supported by a Robert A. Welch Distinguished Chair in Chemistry.

[3] To whom correspondence should be addressed: Dept. of Biochemistry, Faculty of Medicine and Dentistry, University of Alberta, Edmonton, Alberta T6G 2H7, Canada. Tel.: 780-492-2136; Fax: 780-492-0886; E-mail: mark.glover@ualberta.ca.

[4] The abbreviations used are: Ub, ubiquitin; DSB, double strand break; MIU, motif interacting with ubiquitin; MEF, mouse embryo fibroblast; SAXS, small angle x-ray scattering; SPR, surface plasmon resonance; ATM, ataxia telangiectasia mutated; MES, minimal ensemble search; PDB, Protein Data Bank; Gy, gray; GAJOE, genetic algorithm judging optimization of ensemble.

although the RNF8 RING tightly binds and activates Ubc13, RNF168 interacts much more weakly with Ubc13 and does not significantly stimulate its catalytic activity (7).

In the DSB response, RNF8 provides an attractive pivot point for the possible control of pathway choice as it acts in recruitment of 53BP1 for non-homologous end joining and BRCA1 for homologous recombination repair. Such pathway choice selection for non-homologous end joining and homologous recombination repair, as demonstrated by dissection-of-function inhibitors for MRE11 exo- and endonuclease (27), has potential value for gene therapy and cancer biology. For these repair factor recruitment functions, a hydrophobic interaction of RING E3 ligases positions the ubiquitin C terminus in an E2 groove for possible activation of the thioester by the incoming acceptor lysine (6, 28–30) and targets the E2 to the site of a substrate. However, it is unknown whether both the E2 stimulating activity and the E2 targeting activity of RING E3 ligases are required for proper functioning of an E2-E3 pair and whether RNF8 stimulates Ubc13 catalytic activity similarly. Here, we show through combined structural, biochemical, mutational, and imaging studies that a RING E3-mediated E2-stimulating mechanism holds true for the RNF8-Ubc13 E3-E2 pair. Using a designed RNF8 mutant specifically deficient in its E2 stimulating activity, we find that the RNF8 E2 stimulating activity is required for proper functioning of the DNA damage response and that the recruitment of an RNF8 mutant unable to stimulate Ubc13-dependent Lys-63 ubiquitination to the sites of DNA DSBs is insufficient for repair. Our collective results indicate that the direct stimulation of Ubc13 polyubiquitination by RNF8 is needed for the formation of Lys-63-linked ubiquitin chains at sites of DNA DSBs and for the downstream recruitment of BRCA1.

Experimental Procedures

Protein Production—Ubc13, Mms2, and RNF8 cloning and protein production/purification were previously described (7, 31). The RNF8 L451D and R441A and Ubc13C87K mutants were made using PCR mutagenesis from wild type RNF8 and Ubc13 templates. The mUBA1 enzyme was produced according to a previously published protocol (32); however, the His tag vector used was pET47b(+).

Crystallization—The formation of a stable E2∼Ub isopeptide bond has previously been described (28) using purified E1, Ubc13C87K, and ubiquitin at pH 10. The RNF8-Ubc13C87K∼Ub complexes were concentrated to 10 mg/ml in a buffer containing 20 mM HEPES, pH 6.8, 200 mM NaCl, 10 μM $ZnSO_4$, and 1 mM DTT. Crystals were grown using vapor diffusion in 0.1 M imidazole, pH 8.0, 1.04 M $(NH_4)_2HPO_4$. Crystals grew within 1–2 weeks.

Structure Solution and Refinement—Both SAXS and crystallography x-ray data were collected at the SIBYLS beamline (12.3.1) at the Advanced Light Source (33). Both experiments were performed at an x-ray wavelength of 1.03321 Å. The data were processed in HKL2000, and structure solution was accomplished using PHENIX (Table 1) (34). A model for molecular replacement was created from a modified version of the previously determined RNF8-Ubc13 structure (PDB code 4ORH). The RING domain (amino acids 392–485) of RNF8 was used, and a second Ubc13 molecule was added using 2-fold symmetry to create a dimer complex. Phaser (35, 36) was used to place two copies of this model within the crystallographic asymmetric unit. Fig. 1*C* shows the density of Ubc13 when it is omitted from the molecular replacement. Next, a ubiquitin (PDB code 4AP4) with a truncated C-terminal tail was used as a second search model. Phaser was able to place a single ubiquitin into this model (Z-score = 6.2) onto a region with significant positive difference density (Fig. 1, *D–G*). Alignment of the RNF8-Ubc13∼Ub structure with the RNF4-UbcH5a∼Ub (PDB code 4AP4) structure revealed that the ubiquitins are in the same relative orientation to the E2-E3 (Fig. 1, *A* and *B*). Weaker difference density was also observed at each of the other potential ubiquitin positions predicted by noncrystallographic symmetry (Fig. 1, *D–G*). NCS was used to position these ubiquitins, and the validity of the placement of each ubiquitin was monitored via changes in R_{free} and visual inspection of the difference density. The addition of each of the ubiquitin chains changed the R_{free} values as follows: A, 0.345 to 0.337; F, 0.335 to 0.334; G, 0.343 to 0.339; and L, 0.343 to 0.344. Fig. 1, *D–G*, corresponds to the difference density of ubiquitin chains A, F, G, and L prior to model introduction, respectively. The additions of ubiquitin chains A and G resulted in the largest reductions in R_{free}, although addition of either ubiquitin chain F or L did not significantly change R_{free}. However, in addition to the positive difference density observed for ubiquitin chains F and L (Fig. 1, *D–G*), the removal of the two chains in a refinement test increased both the R_{free} (0.3262 increase to 0.3283) and R_{work} (0.3179 increase to 0.3256) values, which supported the inclusion of these chains in the final model. Portions of each of the RNF8 coiled coils were placed through alignments with PDB code 4ORH. In one complex, the positive difference density enabled placement of the entire coiled coil (342/345–392), creating crystal contacts between adjacent helical arrays of complexes running down the 6-fold screw axis of the cell. In the

TABLE 1
X-ray diffraction data collection and refinement statistics

	RNF8/Ubc13∼Ub
Data collection	
Space group	P6422
Cell dimensions	
a, *b*, *c* (Å)	341.4, 341.4, 113.4
α, β, γ (°)	90, 90, 120
Resolution (Å)	49.3–8.3 (8.5–8.3)[a]
R_{sym}	11.7 (83.4)[a]
$I/\sigma I$	24.3 (6.6)[a]
Completeness (%)	99.8 (97.9)[a]
Redundancy	21.8 (24.2)[a]
R_{pim}	0.037 (0.162)[a]
$CC_{1/2}$	0.999 (0.973)[a]
Refinement	
No. of unique reflections	4087
R_{work}/R_{free}	32.9/33.7
No. of atoms	
Total	9620
Protein	9612
Ligand/ion	8
Water	0
Overall *B*-factor	522.7
Protein	522.7
Ligand/ion	498.9
Root mean square deviations	
Bond lengths (Å)	0.007
Bond angles (°)	1.09

[a] Values in parentheses indicate the highest resolution shell.

second complex, rotated 180° to the first, the coiled coils are pointing into a large solvent channel running down the interior of the helical filament. The positive difference density for these coiled coils only justified modeling a small section of the coiled coil corresponding to residues 380–392. The junction where the coiled-coil C-terminal residue (392) is linked to the N-terminal RING residue (393) was real space refined in Coot using Ramachandran restraints to maintain the bonds and angles. RNF8 and Ubc13 were treated as separate rigid bodies, and there was little movement relative to each other, which maintained the RNF8-Ubc13 binding interface, although the ubiquitin molecules were each treated as separate units in rigid body refinement. This allowed the ubiquitin molecules to move as rigid bodies relative to the RNF8-Ubc13 complexes.

SAXS Data Collection and Analysis—Because of the previous observation that another lysine residue (Lys-92) in the Ubc13 active site is modified using the isopeptide formation protocol, we made the same stable mutation (K92A) as Branigan *et al.* (37) to prevent nonspecific modification for the SAXS. Thus, when Ubc13~Ub is used as a shorthand to describe the ubiquitin-conjugated Ubc13, it is Ubc13C87K, K92A, conjugated with ubiquitin for the SAXS data. The WT and L451D RNF8-Ubc13~Ub complexes with and without Mms2 were concentrated to ~6 and 4 mg/ml. The flow-through buffer was collected after sample concentration and used for buffer subtraction. SAXS data were collected on a Pilatus 2M detector, although other parameters were held consistent as reported previously (38, 39). ScÅtter and Primus (40) were used to determine which data sets of various exposure times were of high quality for further analyses (*i.e.* showed little to no aggregation or interparticle interference). The lower (~4 mg/ml) concentrations provided the best data at the lowest exposure time of 0.5 s. Primus was used to determine R_g and D_{max} for all data sets. Because of the elongated nature of the dimer RNF8-Ubc13~Ub/Mms2 complex, a smaller q-range limit for the Guinier approximation was used ($qR_g < 0.8$), instead of the limit for more globular proteins/complexes ($qR_g < 1.3$), to determine R_g, which resulted in fewer data points for the approximation (41). The extrapolation to $I(0)$ at low q was determined in Primus, using GNOM (42). BILBOMD (43) was used for molecular dynamics simulations to generate model libraries by choosing a range of R_g values with 600 conformations per R_g step. The N- and C-terminal tails of Ubc13, RNF8, ubiquitin, and Mms2 were left flexible relative to the rigid bodies of the complexes. Ubiquitin was flexibly tethered to Ubc13 active site. FoXS (44, 45) was used for calculating theoretical scattering curves and a minimal ensemble search (MES), which is further discussed under "Results." GAJOE is part of the EOM 2.0 suite of SAXS analysis software (46), and with the FOXS-generated theoretical scattering curves, it was used to find ensemble fits to all data sets.

Surface Plasmon Resonance—0.19 pmol/mm^2 of Ubc13 was coupled to a CM5 BIAcore sensor chip using an amine coupling kit. Briefly this included activation with *N*-hydroxysuccinimide/*N*-ethyl-*N*′-(3-dimethylaminopropyl)-carbodiimide hydrochloride for 7 min at a flow rate of 5 μl/min, conjugation of 1 μM purified Ubc13 in 10 mM sodium acetate, pH 5, at a flow rate of 5 μl/min, and blocking with 1 M ethanolamine, pH 8.5, for 7 min at a flow rate of 5 μl/min. The purified RNF8 proteins were diluted to 10 μM in 10 mM HEPES, pH 7.4, 150 mM NaCl, 0.005% Nonidet P-40 at a flow rate of 30 μl/min, and a titration series from 0 to 10,000 nm was performed on a BIAcore 3000 SPR biosensor. Control samples of buffer only were used for blank subtraction. Because of the rapid kinetics, estimated apparent equilibrium dissociation constants (K_D) were determined using a fractional saturation analysis in SigmaPlot. The response used for the steady state affinity calculation was 20 s after the injection start to avoid background RNF8 binding effects at higher concentrations.

Ubiquitination Assay—All ubiquitination assays were done essentially as described previously (47). The reactions were run for 15, 30, 45, and 90 min at 37 °C and quenched with SDS-PAGE loading buffer, and the results were visualized by Western blotting. The primary antibody was anti-ubiquitin (Santa Cruz Biotechnology: host, mouse; catalogue no. sc-166553; lot no. F2012), and the secondary was anti-mouse FITC (Sigma: host, goat; catalogue no. F0257).

Generation of Stably Integrated RNF8 MEFs—The generation of RNF8 knock-out mouse embryonic fibroblasts has previously been described (48). Re-introduction of either WT or L451D RNF8 was accomplished using retroviral transduction. 293T cells were transiently transfected with 0.9 μg of gag/pol expression vector (64), 0.1 μg of VSV-G envelope vector, and 1 μg of pBABE-hygromycin-HA~RNF8 transfer vector using Qiagen Effectene for viral production. Viral supernatant was collected at 24, 48, and 72 h post-transfection. Knock-out MEFs were infected twice with the viral supernatants. HA~RNF8-expressing cells were selected with 400 μg/ml hygromycin.

Immunoprecipitation Assay—Extracts were prepared from RNF8 knock-out mouse embryonic fibroblasts transfected with HA-tagged RNF8 WT or RNF8 L451D constructs. 24 h after transfection, extracts that contained detergent-soluble RNF8 in NETN (20 mM Tris, pH 7.5, 150 mM NaCl, 1 mM EDTA, and 0.5% Nonidet P-40, mixture protease inhibitor) were prepared. Extracts were pre-cleared, incubated with anti-HA antibody for 4 h at 4 °C, and washed twice with extraction buffer. Immunocomplexes were eluted by boiling in SDS sample buffer for 5 min. A primary antibody was used to stain for RNF8 (Abnova: host, mouse; catalogue no. H00009025-B01P; lot no. 09117WUIZ).

DNA Damage Localization Assays with Stable Cell Lines—Transduced MEF cells or knock-outs were seeded to 1×10^4 cells per well in a 96-well glass bottom plate the day before using a hemocytometer. The next day cells were irradiated with 3 Gy ionizing radiation and were allowed to recover for 0.5, 1, and 2 h before fixation and immunofluorescence. The primary antibodies used were anti-HA (Covance: host, mouse; catalogue no. MMS-101R; lot no. E11EF01029), anti-Lys-63 ubiquitin chains (Millipore; host, rabbit; catalogue no. 05-1308; lot no. 2517822), anti-53BP1 (Santa Cruz Biotechnology: host, rabbit; catalogue no. sc-22760; lot no. 12010), and anti-γH2AX (Millipore: host, mouse; catalogue no. 05-636; lot no. 2535296). Proteins were visualized with anti-mouse Cy3-conjugated secondary antibody (The Jackson Laboratory: host, goat; catalogue no. 115-165-146) and an anti-rabbit Alexa Fluor 488 secondary antibody (Molecular

Probes: host, goat; catalogue no. A11034). Images were acquired using a High Content Instrument (Molecular Devices MetaXpress XLS). A *Z*-stack was taken for each image using either 1- or 0.6-μm steps. Image analysis was accomplished using a foci count and colocalization module in CellProfiler (49, 50), with restraints optimized to detect empirically determined foci, while minimizing false positives from background stain. Data were analyzed using Microsoft Excel 2010. Statistical significance was determined with a two-tailed Student's *t* test and significance level of *, $p < 0.005$.

Immunofluorescence Staining with Transiently Transfected Cells—RNF8 knock-out MEFs were transfected with the indicated constructs using Lipofectamine® 3000 Reagent according to the manufacturer's protocols. Cells were irradiated with 2–5 Gy of ionizing radiation and allowed to recover as indicated. Cells were permeabilized prior to fixation in a buffer containing 20 mM HEPES, pH 7.9, 150 mM NaCl, 300 mM sucrose, 3 mM $MgCl_2$, 0.5% Triton X-100 for 5 min on ice. Cells were fixed with 4.0% paraformaldehyde in PBS, pH 7.5, for 20 min at room temperature. Cells were permeabilized with PBS containing 0.5% Triton X-100 for 5 min. Next, cells were washed twice with PBS, inverted onto 30-μl aliquots of an appropriate primary antibody, and incubated at room temperature for 60 min. Coverslips were rinsed with PBS containing 0.1% Triton X-100 and washed twice with PBS before a 30-min incubation with an appropriate secondary antibody conjugated to a fluorophore. Cells were rinsed with PBS containing 0.1% Triton X-100 and washed twice with PBS. Coverslips were mounted onto slides containing ~10 μl of a 90% glycerol/PBS-based medium containing 1 mg of *para*-phenylenediamine/ml and 0.5 μg of DAPI/ml. A panel of commercially available primary antibodies directed against various DNA damage proteins, 53BP1 (same as mentioned previously), BRCA1 (Santa Cruz Biotechnology; host, mouse; catalogue no. sc-6954; lot no. L1009), FK2 (Enzo, Inc.: host, mouse; catalogue no. PW8810; lot no. X17691), and MDC1 (Novus Biologicals: host, rabbit; catalogue no. NB100-395; lot no. A2), were used to detect colocalization of these proteins at the break sites. Proteins were visualized with anti-rabbit Cy3-conjugated secondary antibody (Molecular Probes: host, goat; catalogue no. 111-165-144) and an anti-mouse Alexa Fluor 488 secondary antibody (Molecular Probes: host, goat; catalogue no. A11001). Cells were observed using a microscope (Axiovert 200 M; Carl Zeiss, Inc.), and composite figures of collected images were assembled in Photoshop CS3 and Illustrator CC (Adobe).

Cell Cycle Analysis—RNF8 knock-out MEFs reconstituted with WT or L451D RNF8 were harvested and fixed in ice-cold 70% ethanol, added dropwise while gently vortexing. After a minimum 60-min fixation on ice, samples were pelleted at 200 × *g* for 10 min at 4 °C, and resuspended in PBS. Cells were then stained with propidium iodide (25 μg/ml in 0.5% bovine serum albumin (BSA) and 0.5 mg/ml RNase A in 1× phosphate-buffered saline (PBS)) for 30 min at 37 °C. The samples were run on an SRII flow cytometer (BD Biosciences) and analyzed using the FACS Diva program (version 6.0) (BD Biosciences).

Results

Crystal Structure of RNF8-Ubc13~Ub Reveals an Activated Ubiquitin Conformation—The E3 RNF4 can stimulate the ubiquitination activity of the E2 UbcH5a by directly interacting with the donor ubiquitin linked to the UbcH5a active site (UbcH5a~Ub) (28, 51). To stabilize the UbcH5a~Ub complex for structural studies, the thioester linkage between the ubiquitin C terminus and the UbcH5a active site cysteine was replaced with an isopeptide linkage via mutation of the active site cysteine to a lysine. To test whether an analogous mechanism may act in the RNF8-Ubc13 system, we employed an isopeptide linkage to covalently tether the ubiquitin C terminus to Ubc13 and crystallized this complex bound to an RNF8 construct encompassing its RING domain and coiled coil (RNF8(345–485)). We previously solved the x-ray crystal structure of RNF8(345–485) bound to Ubc13-Mms2 (7). Here, we crystallized the RNF8(345–485)/Ubc13~Ub complex and determined its structure at 8.3 Å resolution by molecular replacement using our RNF8-Ubc13 and free ubiquitin as search models (see under "Experimental Procedures" and Fig. 1). The limited resolution is likely due to weak contacts between crystallographically related complexes mediated by the flexible RNF8 coiled coils. Despite the low resolution, the difference density after molecular replacement with an RNF8-RING-Ubc13 model (Fig. 1*C*) was sufficient for Phaser to place one ubiquitin molecule, and the other ubiquitins were placed using symmetry operations and rigid body refinement (see under "Experimental Procedures"). There is variability in the difference density for each ubiquitin, which is likely due to the limited crystal contacts in the spaces where they reside (Fig. 1, *D–G*). The resulting structure shows that both RNF8 protomers in the dimer can simultaneously bind a Ubc13~Ub (*i.e.* the RNF8 dimer is doubly loaded), which supports and extends our previous determination of the stoichiometry of the complex in solution (Fig. 1*A*) (7).

Importantly, the structure reveals a ubiquitin conformation that makes contacts with both protomers of the RNF8 RING dimer and the Ubc13 and is hereafter referred to as the closed conformation (Fig. 1*A*). The closest contact between RNF8 and the ubiquitin is between the C-terminal end of the ubiquitin α-helix and the distal RNF8 protomer Leu-451. RNF8 H420 may hydrogen bond with ubiquitin Glu-34 at the α-helix C terminus, as there is an analogous interaction between RNF4 H160 and ubiquitin (28). The canonical hydrophobic Ile-44 patch on ubiquitin, which mediates many ubiquitin interactions with protein partners (52), likely makes contact with the Ubc13 central crossover helix (α2). The ubiquitin orientation resembles that seen in the high resolution RNF4-Ubc13~Ub and RNF4-UbcH5a~Ub structures (Fig. 1*B, middle* and *right panels*). The C-terminal tail of ubiquitin is not modeled, due to weak electron density, but is tethered to Ubc13 via an isopeptide bond with the amino group of the Cys to Lys active site mutation (C87K). The asymmetric unit contains two doubly loaded complexes, and the RNF8 coiled coils are only partially modeled in one of these complexes, likely due to a lack of crystal contacts at their N-terminal end (data not shown). However, the closed ubiquitin conformation is clear.

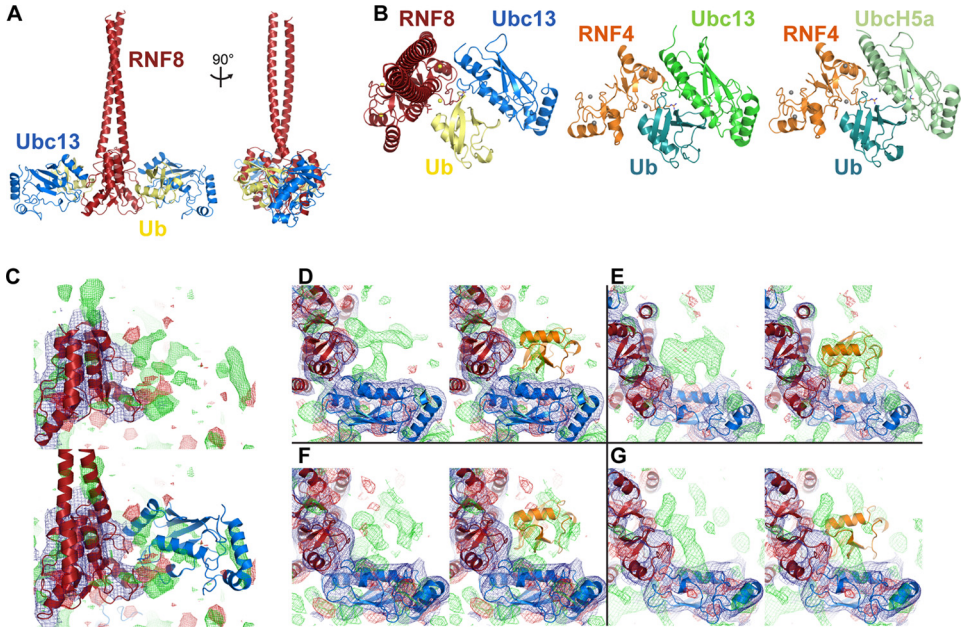

FIGURE 1. **RNF8-Ubc13∼Ub structure and comparison with RNF4-UbcH5a∼Ub.** *A,* overview of RNF8-Ubc13∼Ub structure (Protein Data Bank accession 4WHV). RNF8 dimers are *firebrick red*; Ubc13s are *blue*; and ubiquitins are *yellow*. *B,* top-down view of singly loaded (one Ubc13 and one ubiquitin) RNF8 dimer (*left*), singly loaded (one Ubc13 and one ubiquitin) RNF4 dimer (*middle*; PDB 5AIU), and singly loaded (one UbcH5a and one ubiquitin) RNF4 dimer (*right*; PDB code 4AP4). RNF4 dimer is *orange*, Ubc13 is *green* in *middle panel*; UbcH5a is *pale green*, and ubiquitin is *aqua green*. *C,* electron density maps of RNF8-Ubc13∼Ub structure phased with an RNF8 dimer plus a single Ubc13. The difference density for the missing Ubc13 and RNF8 coiled coil is shown with a full RNF8 and Ubc13 model overlaid in the *bottom panel*. *D–G,* electron density maps for RNF8-Ubc13∼Ub with difference density prior to the introduction of ubiquitin chain A (*D*), chain F (*E*), chain G (*F*), or chain L (*G*) (*left panels* show ubiquitin density only; *right panels* show ubiquitin models in *orange*). For all maps, $F_o - F_c$ difference density contoured at $\sigma = 2$ is shown in *green* and *red*, and $2F_o - F_c$ contoured at $\sigma = 1$ is shown in *blue*.

RNF8 Leu-451 Is Required for Full Stimulation of Ubc13 Catalytic Activity in Vitro—We sought to uncover mutations that destabilize the ubiquitin-RNF8 interface that controls ubiquitin conformation to test its importance for ubiquitination. An alignment of the RNF8-Ubc13∼Ub structure with the high resolution RNF4-Ubc13∼Ub and RNF4-UbcH5a∼Ub structures helped us to infer important residues in RNF8 that mediate the contact with ubiquitin (Fig. 2*A*). Based on these aligned structures, we reasoned that two residues could be largely responsible for stabilizing ubiquitin in the closed conformation. RNF8 Leu-451 makes hydrophobic contacts with the C terminus of the ubiquitin α-helix (Fig. 2*A*). The RNF4-Ubc13∼Ub and RNF4-UbcH5a∼Ub structures make an analogous contact between RNF4 Tyr-193 and the ubiquitin α-helix (28, 37). RNF4 Tyr-193 not only contacts ubiquitin but also forms part of the E3 dimer interface (51); however, our structure predicts that Leu-451 in RNF8 likely does not participate in the RNF8 dimer interface, which is supported by previously determined high resolution RNF8 structures. The second residue is RNF8 Arg-441, which we predict makes hydrogen bonds with both Ubc13 and ubiquitin based on the analogous RNF4 Arg-181 of the RNF4-Ubc13∼Ub (Fig. 2*A*, *left panel*) and RNF4-UbcH5a∼Ub (Fig. 2*A*, *right panel*) structures (28, 37). It has already been shown that mutation of RNF4 R181 to alanine severely impairs RNF4-UbcH5a catalytic activity in a single-turnover assay (51).

To test our hypothesis that RNF8 residues Leu-451 and Arg-441 are largely responsible for ubiquitin conformational selection and stimulation of Ubc13 catalytic activity, we made the RNF8 mutations L451D and R441A. The L451D mutation introduces a negative charge in place of the hydrophobic leucine, which is predicted to repel the carbonyl oxygens at the C terminus of the ubiquitin α-helix to disfavor the closed ubiquitin conformation. The R441A mutant is predicted to disrupt hydrogen bonding RNF8 interactions to Ubc13 and ubiquitin. We tested the ability of these mutants to stimulate Lys-63-linked ubiquitin chain formation by Ubc13-Mms2 compared with wild type RNF8 in an *in vitro* auto-ubiquitination assay using purified proteins (Fig. 2*B*). Under these reaction conditions, Ubc13-Mms2 is able to drive formation of di-ubiquitin; however, addition of wild type RNF8 stimulated the formation of higher order ubiquitin conjugates and chains. The L451D mutation caused a drastic decrease in the ability of RNF8 to stimulate Ubc13; ubiquitination is modestly better than Ubc13-Mms2 alone (Fig. 2*B*, *right panel*). Surprisingly, the R441A mutant had little effect on ubiquitination. To ensure that the mutations only affect ubiquitin conformational selection and not binding to Ubc13, we measured the steady state affinities of the WT and mutant RNF8 proteins for Ubc13 by surface plasmon resonance (Fig. 3*A*). The results demonstrate that the L451D mutation has little effect on the apparent equilibrium dissociation constant ($K_{D,\,\mathrm{WT}}$ ∼1.6 μM; $K_{D,\,\mathrm{L451D}}$ ∼3.4 μM), and the R441A mutation had a very minor effect ($K_{D,\,\mathrm{R441A}}$ ∼4.9 μM). The bivalent binding capability of the RNF8 RING dimer likely increased the apparent on-rate of binding to Ubc13, which suggests that the true affinities are likely lower. This would make the affinities more consistent with other E2:E3 RING pairs such as the monomeric gp78 RING:Ube2g2 complex with a K_D ∼144 μM (53). Taken together, these results indicate that RNF8 L451D selectively abrogates Ubc13-mediated ubiquitination through disruption of RNF8-ubiquitin interactions. The SPR binding data are further supported by

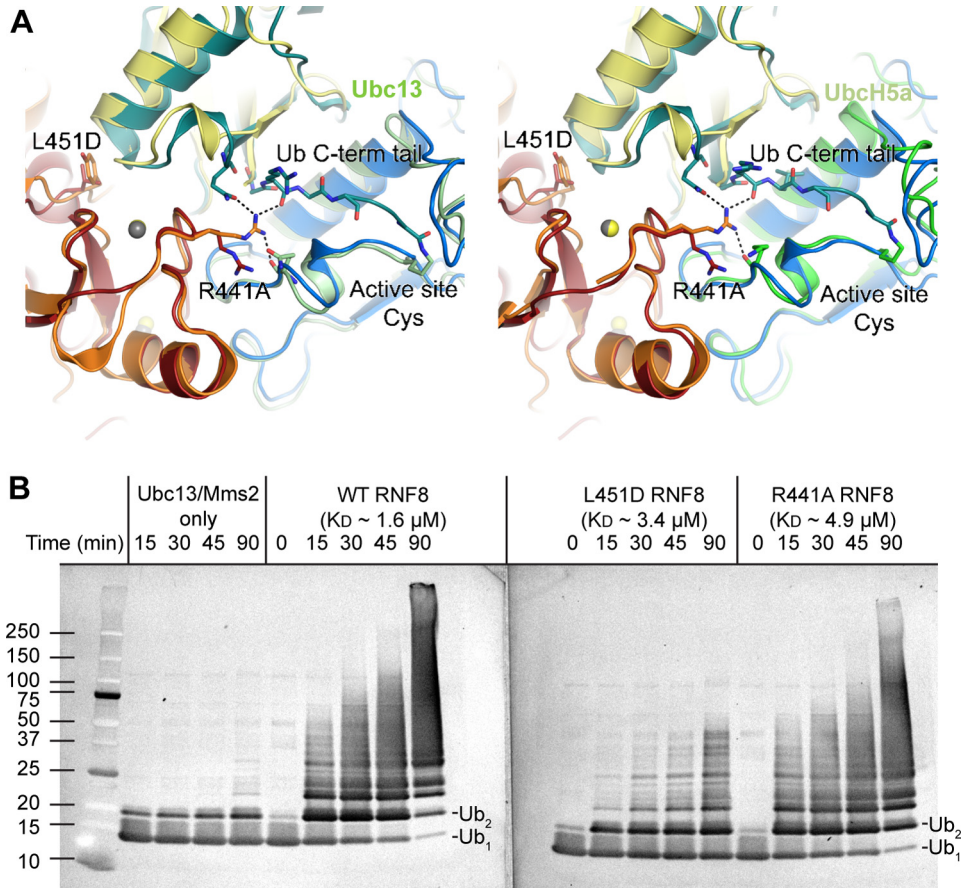

FIGURE 2. **RNF8 mutations affect Ubc13 catalytic activity.** *A,* close-up view of an alignment of the RNF8-Ubc13~Ub structure (RNF8 is *firebrick red*; Ubc13 is *blue*, and ubiquitin is *yellow*) with the RNF4-Ubc13~Ub (PDB code 5AIU; RNF4 is *orange*, Ubc13 is *pale green*, and ubiquitin is *aqua green*) and RNF4-UbcH5a~Ub structure (PDB code 4AP4; RNF4 is *orange*, UbcH5a is *pale green*, and ubiquitin is *aqua green*). Residues proposed to be important for interactions between the E2s, E3s, and ubiquitin are shown as *sticks*; note that side chain residues in the RNF8-Ubc13~Ub complex are inferred from higher resolution structures (PDB codes 4AYC and 5AIU). *B, in vitro* ubiquitination assays in which purified RNF8 (WT, L451D, or R441A) was incubated with Ubc13/Mms2, ubiquitin, ATP, and E1 enzyme for the indicated time before quenching. Results were visualized via Western blotting using an anti-ubiquitin antibody. Mono- and diubiquitin species are indicated. The approximate dissociation constants (K_D) for the interactions of each of the RNF8 proteins with Ubc13 as determined by SPR are indicated.

analytical size exclusion chromatography experiments (Fig. 3*B*).

SAXS Analyses of WT and L451D RNF8-Ubc13~Ub Complex with and without Mms2 Show Ubiquitin Conformational Selection in Solution—We wished to determine whether the closed ubiquitin conformational selection seen in our RNF8-Ubc13~Ub crystal structure is also present in solution and whether the L451D mutation shifts the population distribution of the flexibly tethered ubiquitin. To do this, we used small angle x-ray scattering (SAXS) to assess the solution structure and dynamics of the purified complexes of WT and L451D (Fig. 4) RNF8(345–485)-Ubc13~Ub without Mms2 and with Mms2 (Fig. 5). As noted under "Experimental Procedures," a double mutant of Ubc13 was used (C87K, K92A) in place of wild type Ubc13, to prevent nonspecific modification of a Ubc13 lysine (K92) close to the active site during isopeptide formation of the C terminus of ubiquitin with Ubc13 C87K, as previously observed (37). Guinier analysis of the scattering of the WT and L451D RNF8(345–485)-Ubc13~Ub and WT and L451D RNF8(345–485)-Ubc13~Ub/Mms2 complexes (data not shown) indicated well behaved samples without significant aggregation and the radii of gyrations (R_g) of ~42.3, 41.9, 55.1, and 51.8 Å, respectively. To assess the degree of flexibility of these complexes in solution, we used a method based on the Porod-Debye law to assess the relative electron density contrast between the scattering particle and the solution and to obtain information on the flexibility of the complex (data not shown) (54). All of the SAXS profiles indicate flexibility within the complexes, regardless of mutation or presence of Mms2. The degree of flexibility is correlated to the rate of decay of the SAXS curve as a function of q (54). A plateau region is observed in the Sibyls plots when plotting the SAXS curves as $q^3 \times I(q)$ *versus* q indicating a q^3 decay. This flexibility value, which is between the q^4 decay typical of a compact particle and q^2 decay of an unfolded one, is consistent with discrete elements of conformational flexibility within all of the complexes. We reasoned that this motion may reflect movement of the covalently bound ubiquitin.

To test the idea that the flexibility of the complexes might be due to the reorientation of the tethered ubiquitin relative to the rest of the complex and that the conformational sampling of the ubiquitin may be different in the presence of wild type *versus* L451D RNF8, we utilized MES and GAJOE (46). These methods aim to identify minimal ensembles of conformations of WT or L451D RNF8-Ubc13~Ub, with and without Mms2, that represent the distributions of structures in solu-

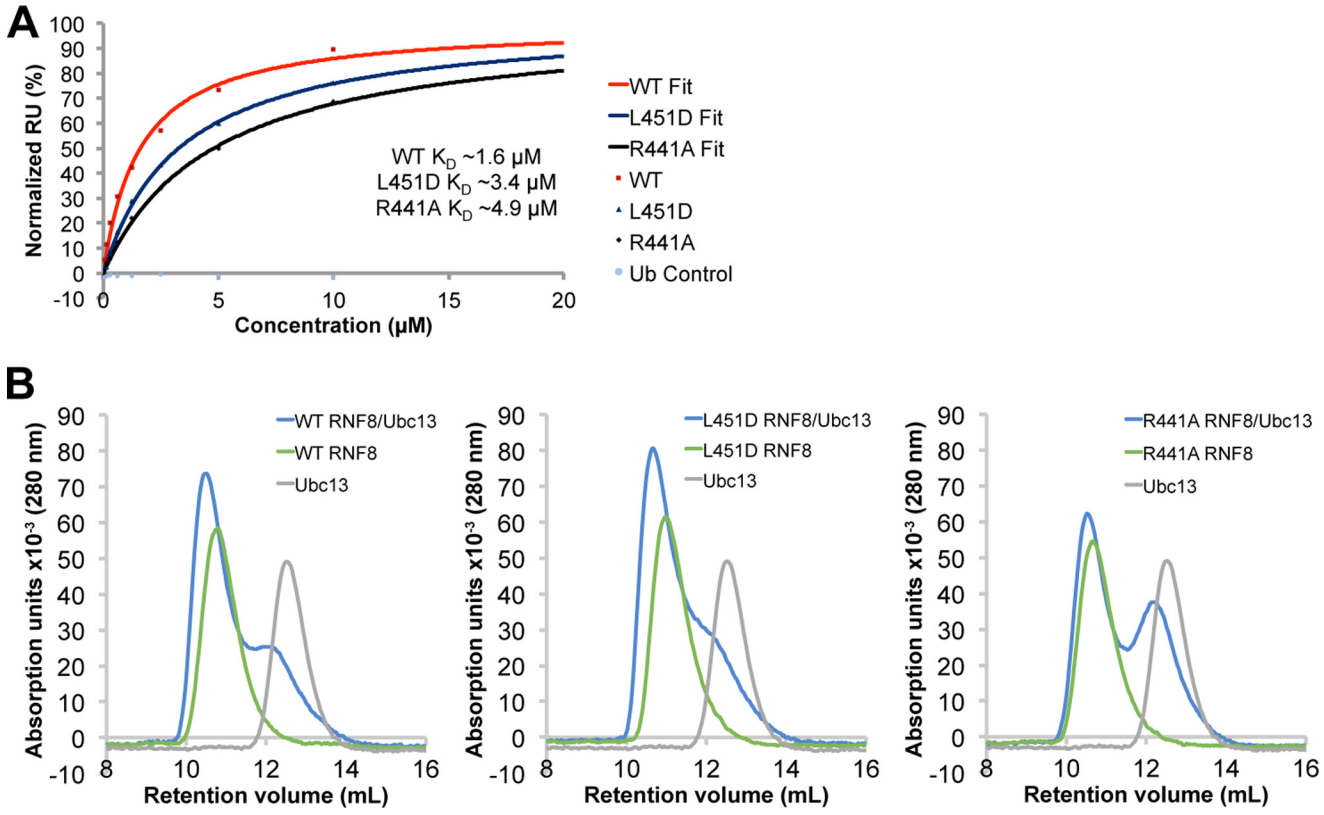

FIGURE 3. **RNF8-ubiquitin interface mutations do not significantly affect binding to Ubc13.** *A,* steady state affinity analysis of the RNF8 SPR curves of WT, L451D, and R441A demonstrating binding to chip-conjugated Ubc13. Ubiquitin was run as a negative control. The saturation point for wild type, L451D, and R441A RNF8 binding to Ubc13 was estimated from a hyperbolic non-linear regression fit to duplicate data sets, and the predicted R_{max} value of each curve was set to 100% for normalization. The response 20 s after the injection start was used for the steady state affinity calculation to avoid background RNF8 binding effects at higher concentrations. The estimated apparent equilibrium constants (K_D) were determined using a fractional saturation analysis (63) in SigmaPlot. *B,* WT, L451D, and R441A RNF8 constructs form complexes with Ubc13 as determined by analytical size exclusion chromatography. Ubc13 and each of the RNF8 constructs were run alone as controls and are overlaid on each of the complex curves.

tion by best fit to the SAXS data. We created a library of stereochemically reasonable RNF8(345–485)-Ubc13~Ub/(±Mms2) models using molecular dynamics as implemented in BILBOMD (43). Using this method, 4740 and 7195 models were generated for the RNF8(345–485)-Ubc13~Ub and RNF8(345–485)-Ubc13~Ub/Mms2 complexes, respectively. The structured bodies of the RNF8 dimer and both Ubc13 and Mms2 molecules were fixed during the simulation, whereas the N- and C-terminal tails were left flexible. Ubc13-tethered ubiquitin was also allowed to sample conformational space. FoXS (44, 45) was used to calculate theoretical scattering curves for each of the models in the library and to perform the minimal ensemble search. These theoretical scattering curves were also used by GAJOE, a different genetic algorithm for analyzing SAXS curves.

The MES approach uncovered ensembles containing five models that nicely fit the data ($\chi^2 < 2$) for each of the complexes (Figs. 4 and 5). Each of the minimal ensembles contained structures in which either one or both ubiquitins are positioned in the closed conformation similar to the crystal structure; however, other structures were also selected in which the tethered ubiquitin is displaced from Ubc13. Interestingly, the complexes containing WT RNF8 consistently displayed a higher proportion of closed conformations compared with the complexes containing the L451D RNF8 mutant, as selected by the genetic algorithm. For the WT RNF8-Ubc13~Ub complex, 51% of the algorithm-selected structures are in the closed state. In contrast, only 29% were in the closed state for the L451D mutant. Similarly for the WT RNF8-Ubc13~Ub/Mms2 complex, 44% of selected complexes were in the closed state, although only 14% were in the closed state in the complex containing the L451D mutant (Fig. 5). Likewise, the GAJOE approach also gave ensembles in which closed ubiquitin conformations were more highly populated in the WT RNF8 complexes compared with the complexes with the L451D RNF8 mutant (data not shown). The discrimination between the closed and non-closed more extended states is largely dictated by scattering in the resolution range between q ~0.1 and 0.2 Å^{-1}. Complexes containing WT RNF8 consistently showed reduced scattering in this range compared with the L451D complexes (Figs. 4*B* and 5*B*). The response of this feature to change in the ubiquitin distribution is quite evident when comparing the overlaid theoretical scattering curves of the individual models to each other in Figs. 4*A* and 5*A* (see *close-up insets*). Together, these data show that the RNF8 L451D mutant primarily changes the fraction of covalently bound ubiquitin in the closed conformational state to impact the Ubc13 stimulating activity of RNF8.

RNF8 L451D Mutation Severely Impairs Lys-63-linked Polyubiquitin DNA Damage Signaling—The RNF8 L451D separation-of-function mutant provides an excellent opportunity to specifically test the role of the Ubc13 stimulating activity of RNF8 in mammalian cells, because the other functions of RNF8, specifically its FHA-dependent recruitment

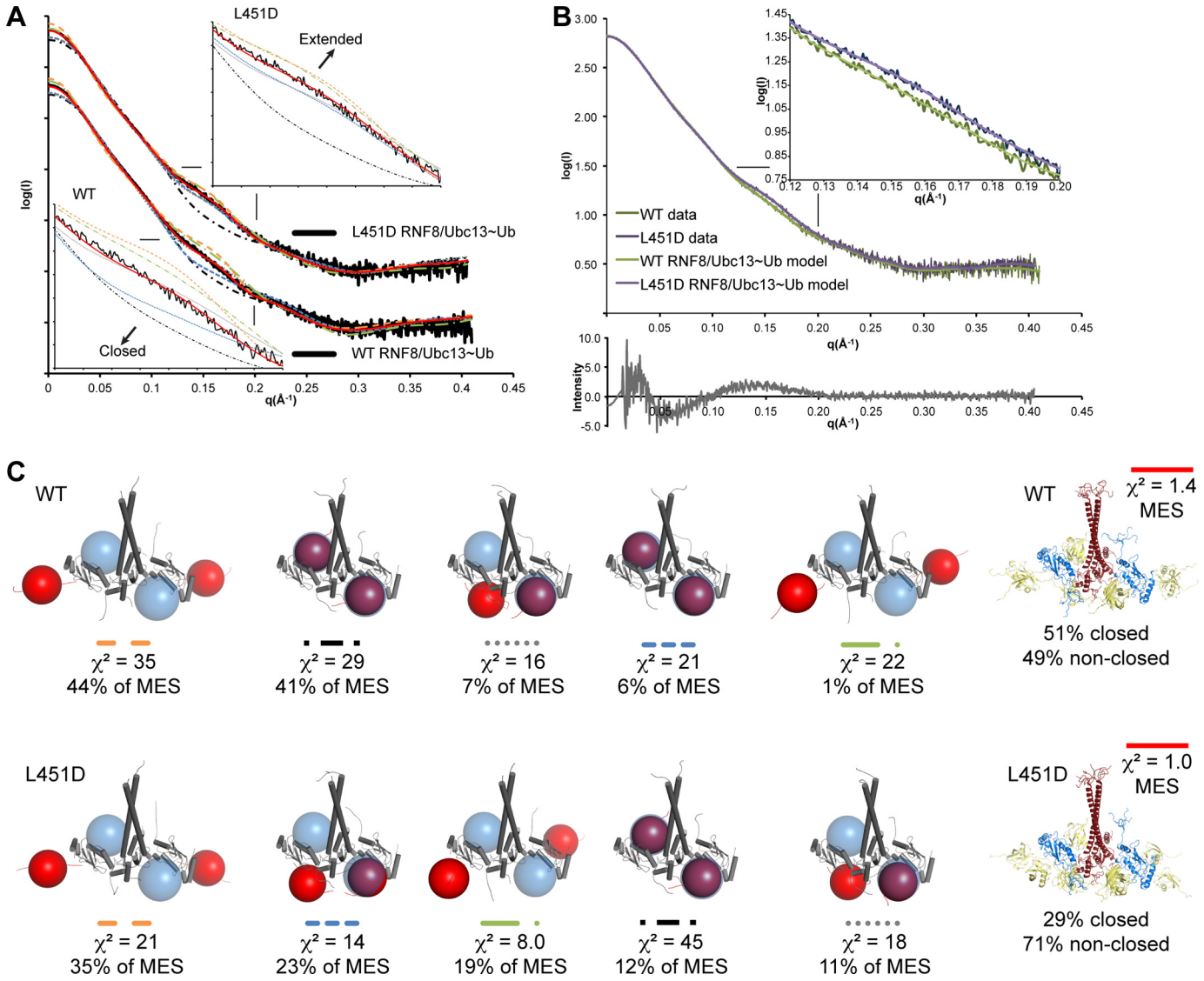

FIGURE 4. **SAXS analysis of WT and L451D RNF8-Ubc13~Ub complexes.** *A,* plot of the extrapolated experimental SAXS curve is shown as a *black solid line*. The selected models that compose the MES ensemble (*red*) are overlaid in various colors and line types. Close-up views between q(Å^{-1}) 0.12 and 0.2 for WT (*bottom left*) and L451D (*top right*) RNF8-Ubc13~Ub of the scattering curves are shown. *B, top panel,* WT and L451D RNF8-Ubc13~Ub SAXS curves were scaled, and lines of best fit were calculated in Primus (*inset panel* is close-up of the $0.12 < q < 0.2$ Å^{-1} region). *Bottom panel* shows a plot of a difference SAXS spectrum in which the scaled intensity of the RNF8 WT complex is subtracted from the scaled intensity of the RNF8 L451D complex. *C,* schematic representations of the individual models that comprise the MES for each complex are shown. *Colored lines* above the models correspond to curves overlaid in *A*. The relative weighting of each model to the overall MES is listed as a percentage, and the goodness of fit (χ^2) of each individual model to the experimental data is indicated. *Blue spheres* represent the closed ubiquitin position, and *red spheres* represent ubiquitin. The *purple spheres* indicate overlapping *blue* and *red* indicating ubiquitin in a closed position. SAXS curves have been deposited to SASBDB: WT RNF8-Ubc13~Ub (SASDBR3); L451D RNF8-Ubc13~Ub (SASDBT3).

and Ubc13 binding activities, should be unaffected in the mutant. To test the impact of decreased RNF8-dependent catalytic stimulation of Ubc13 on DNA damage signaling, we retrovirally reintroduced full-length WT or L451D hemagglutinin (HA)-tagged RNF8 into RNF8 knock-out mouse embryonic fibroblasts (RNF8$^{-/-}$ MEFs), subjected the cells to ionizing radiation to induce DNA damage, and imaged protein localization in the DNA damage response by immunofluorescence (Figs. 6–8). The RNF8 proteins produced in these stable cell lines were expressed at similar levels, maintained Ubc13 binding (Fig. 6, *A* and *B*), and colocalized with γH2AX (Fig. 6*C*), demonstrating that the L451D mutation does not impair RNF8 recruitment to sites of DNA damage. Additionally, we found that MEFs reconstituted with RNF8 L451D showed little change in cell cycle progression compared with MEFs reconstituted with RNF8 WT (Fig. 6*D*). To test the effects on Lys-63-linked ubiquitin chain formation of the L451D mutation, we performed immunofluorescence in these cells with an antibody specific to Lys-63-linked polyubiquitin and hemagglutinin-tagged RNF8. The results indicate that although the WT RNF8 associated with DNA damage foci together with Lys-63-linked polyubiquitin, the degree of colocalization of these foci with RNF8 was dramatically reduced in the L451D mutant (Fig. 7, *A* and *B*). These results indicate that although the RNF8 L451D mutant is able to localize to DNA damage foci, it markedly reduces the formation of Lys-63-linked polyubiquitin within these foci.

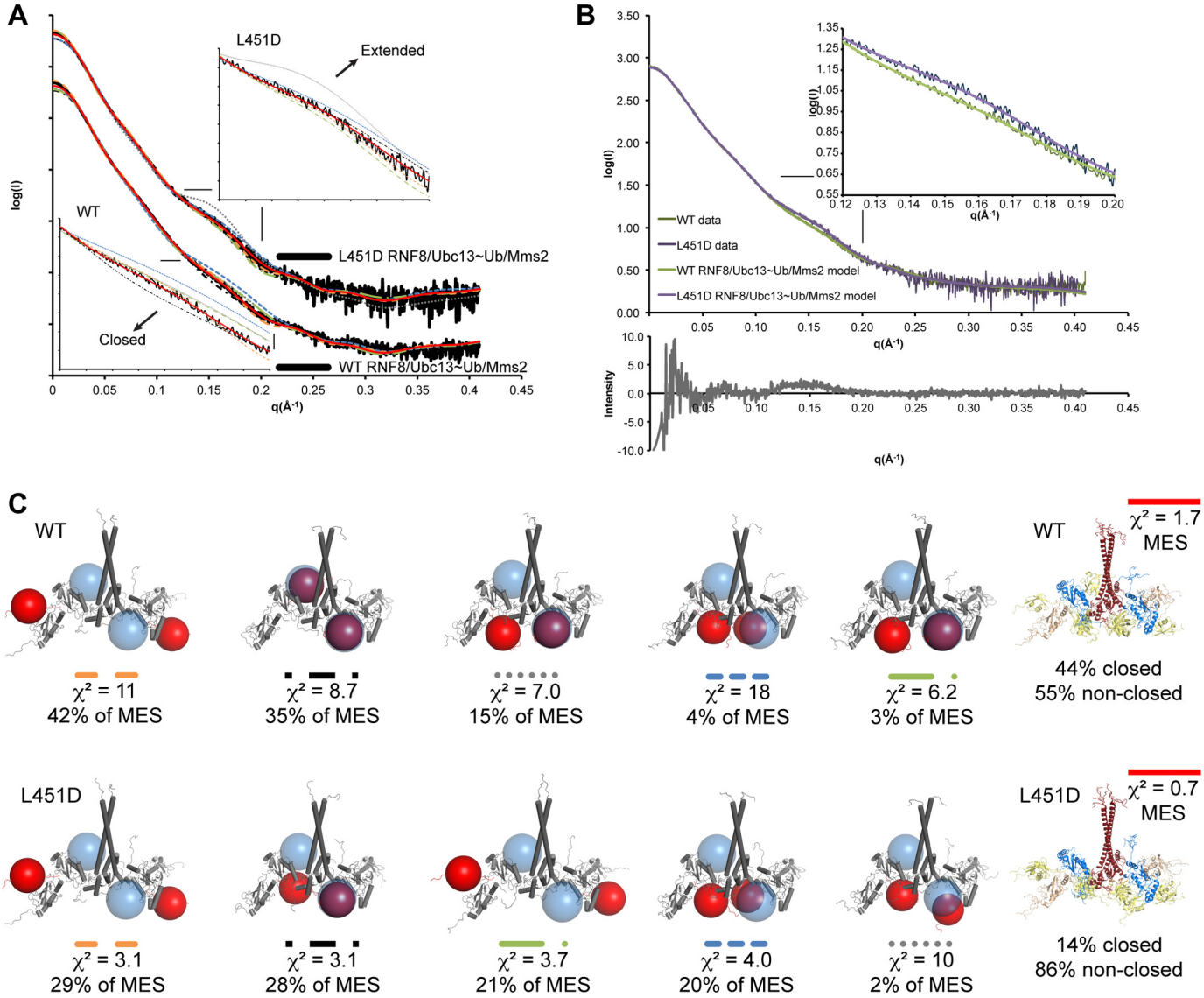

FIGURE 5. **WT and L451D RNF8-Ubc13~Ub/Mms2 complex SAXS curve analysis.** *A,* plot of the extrapolated experimental SAXS curve is shown as a *black solid line*. The selected models that compose the MES ensemble (*red*) are overlaid in various colors and line types. Close-up views between q(Å^{-1}) 0.12 and 0.2 for WT (*bottom left*) and L451D (*top right*) RNF8-Ubc13~Ub/Mms2 of the scattering curves are shown. *B, top panel,* WT and L451D RNF8-Ubc13~Ub/Mms2 SAXS curves were scaled, and lines of best fit were calculated in Primus (*inset panel* is a close-up of the $0.12 < q < 0.2$ Å^{-1} region). *Bottom panel* shows a plot of a difference SAXS spectrum in which the scaled intensity of the RNF8 WT complex is subtracted from the scaled intensity of the RNF8 L451D complex. *C,* schematic representations of the individual models that comprise the MES for each complex are shown. *Colored lines* above the models correspond to curves overlaid in *A*. The relative weighting of each model to the overall MES is listed as a percentage, and the goodness of fit (χ^2) of each individual model to the experimental data is indicated. *Blue spheres* represent the closed ubiquitin position, and *red spheres* represent ubiquitin. The *purple spheres* indicate overlapping *blue* and *red* indicating ubiquitin in a closed position. SAXS curves have been deposited to SASBDB: WT RNF8-Ubc13~Ub/Mms2 (SASDBS3); L451D RNF8-Ubc13~Ub/Mms2 (SASDBU3).

To further test the biological importance of the Ubc13 stimulating activity of RNF8, we probed the effects of the inhibition of RNF8-dependent polyubiquitination on the downstream DNA damage signaling factors, 53BP1 and BRCA1, as well as ubiquitin conjugates (via FK2, an antibody that detects mono- and polyubiquitin conjugates) by monitoring the association of these proteins with IR-induced DNA damage foci by immunofluorescence (Figs. 8 and 9) (12, 55). Consistent with previous reports, we found that ionizing radiation-induced 53BP1, BRCA1 and FK2 foci were severely impaired in RNF8 knockout MEFs (12, 55). Reintroduction of WT RNF8 into these cells rescued IR-induced 53BP1 foci formation (Fig. 8), as well as BRCA1 and FK2 foci formation (Fig. 9*B*). Strikingly, reintroduction of RNF8 L451D did not restore 53BP1, BRCA1, and FK2 foci formation. These results highlight the importance of the Ubc13 stimulating activity of RNF8 and uncouple it from its FHA-dependent recruitment to sites of DNA damage.

Chromatin Targeting of RNF168 to Sites of DNA Damage Bypasses the Requirement of RNF8 for 53BP1 but Not FK2 or BRCA1 Foci Formation—We then wished to determine the role of RNF8 in RNF168-mediated ubiquitin signaling in DSB repair. In the canonical RNF8/RNF168 pathway, the FHA domain of RNF8 binds to ATM-phosphorylated MDC1 to link the phosphorylation cascade to the ubiquitination cascade (12, 55). A recent study suggests that RNF8-Ubc13 then ubiquitinates H1-type linker histones (possibly *de novo* or previously

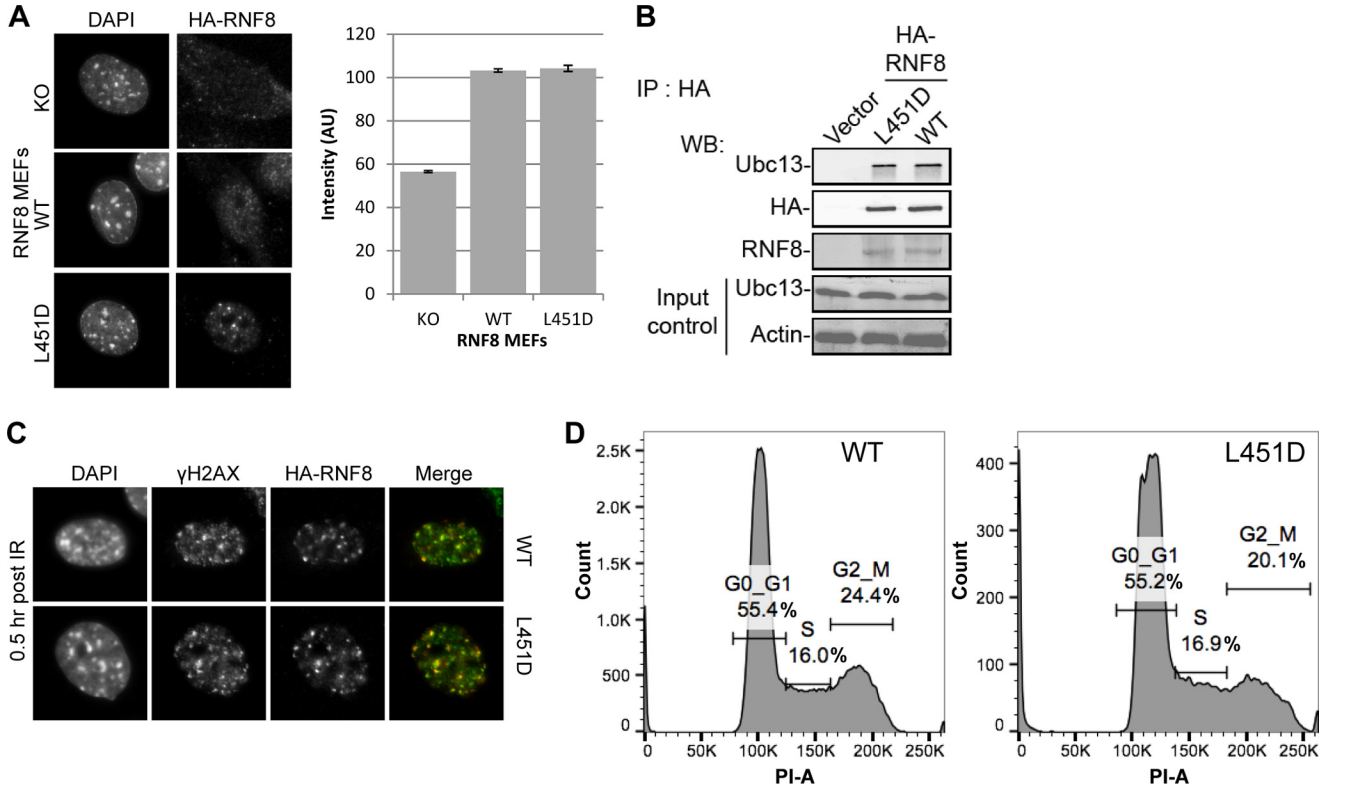

FIGURE 6. **RNF8 levels are similar in the WT and L451D MEF populations.** *A,* anti-HA antibody was used to stain RNF8 knock-out (*KO*), WT, and L451D MEFs (*left panel*). The nuclear intensity of HA-RNF8 was quantified in arbitrary units (*AU*) (*right panel*). The nonspecific nuclear HA stain of the KO cells was used to determine a threshold to filter out any non-reconstituted cells, and the nuclear intensity of HA-RNF8 was quantified for the remaining WT and L451D MEFs. The tonal range of cell images was rescaled from 0 to 255 in Photoshop to increase the overall contrast for display in the representative image. *B,* immunoprecipitation using an anti-HA antibody to detect WT or L451D HA-RNF8 in complex with endogenous Ubc13. The HA-tagged RNF8 wild type (*WT*) or L451D (L451D) were expressed in RNF8 knock-out mouse embryonic fibroblasts, and their interaction was measured by immunoprecipitation with anti-HA antibody followed by immunoblotting with the indicated antibodies. The tonal range of whole images was rescaled from 0 to 255 to increase the overall contrast for display. *C,* γH2AX/RNF8 colocalized foci 0.5 h after ionizing radiation in both wild type and L451D RNF8 reconstituted MEFs. RNF8 foci are *red,* and γH2AX are *green* in the merged images. The tonal range of whole images was rescaled from 0 to 255 in Photoshop to increase the overall contrast for display. *D,* DNA content of wild type and L451D RNF8 reconstituted MEFs was analyzed via propidium iodide staining and flow cytometry. The percentages of cells in G_0/G_1, S, and G_2/M phases are indicated. At least 20,000 cells per cell line were measured and analyzed.

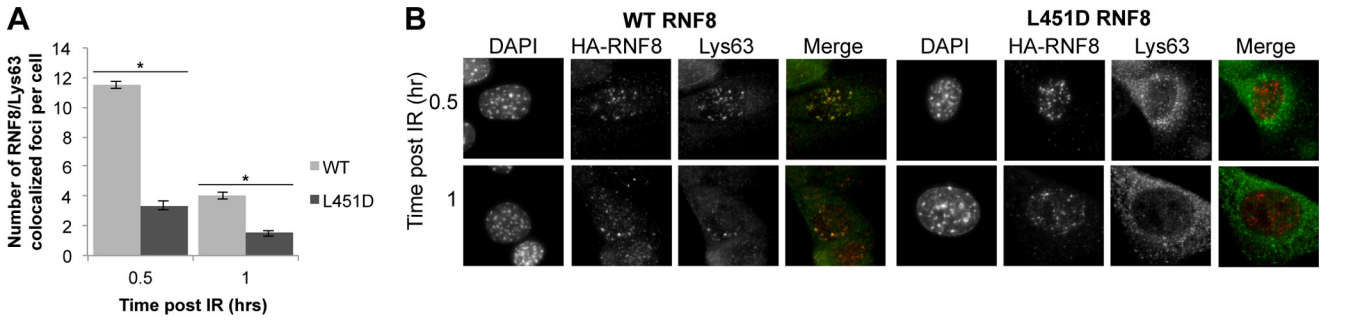

FIGURE 7. **RNF8 L451D mutation sharply reduces Lys-63-linked polyubiquitin chain formation in MEF cells.** *A,* RNF8/Lys-63 colocalized foci per cell for WT or L451D cells from 0.5 to 1 h post 3 Gy of ionizing radiation. *B,* representative image of the RNF8 L451D mutation on DNA DSB repair via an RNF8/Lys-63 IRIF time course. Wild type RNF8 reconstituted MEFs are in the *left panel* and L451D RNF8 MEFs are in the *right panel*. RNF8 is *red,* and Lys-63 is *green* in the merged images. The tonal range of cell images was rescaled from 0 to 255 in Photoshop to increase the overall contrast for display. Cells with ≥20 RNF8 foci per cell were examined to ensure only RNF8-positive cells were analyzed, to avoid inclusion of spurious non-IR induced foci, and increased diffuse background stain in later time points. The experiment was done in triplicate, and data were pooled with at least 200 cells per time point, and standard error of the mean is included. *, $p < 0.005$ comparing WT and L451D for each time point using a two-tailed Student's *t* test.

monoubiquitinated) with short Lys-63 ubiquitin chains, recruiting RNF168 through its MIU domains (23). RNF8 and/or RNF168 extend the Lys-63-linked polyubiquitin chains that are required for RAP80, BRCA1, and FK2 foci formation. RNF168 then monoubiquitinates histone H2A on lysine 15, which in turn recruits 53BP1. To determine the biological role of RNF8 in RNF168-mediated DNA damage response, we targeted RNF168 to DNA damage sites independent of Lys-63 ubiquitin chains by fusing the BRCT domain of MDC1 (binds phosphorylated H2AX) to RNF168 lacking the MIU ubiquitin-targeting motifs (GFP-RNF168-dMIU-BRCT) (Fig. 9). Chimeric constructs were transfected into $RNF8^{-/-}$ MEFs, which cannot form Lys-63 ubiquitin chains, but allow Ub-H2A K15 activity to be restored while eliminating the Lys-63-linked polyubiquitin

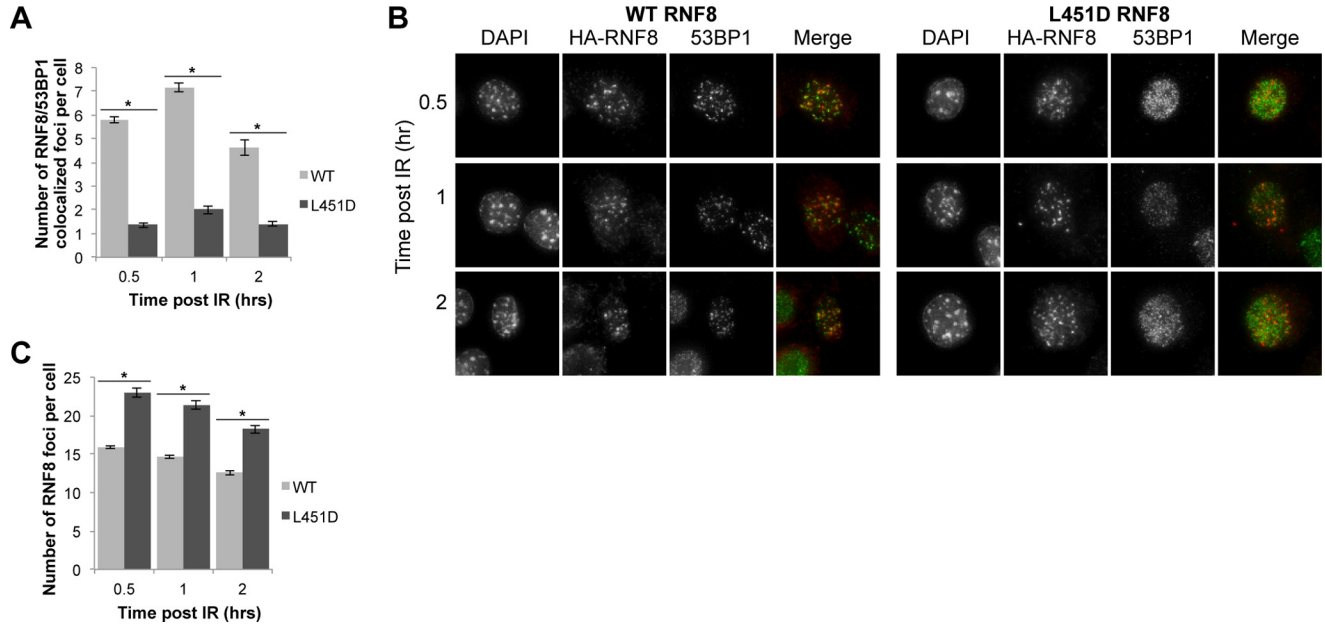

FIGURE 8. **Effects of the RNF8 L451D mutation on DNA DSB repair via a RNF8/53BP1 IRIF time course.** *A,* RNF8/53BP1 colocalized foci per cell for WT or L451D cells from 0.5 to 2 h post 3 Gy of ionizing radiation. *B,* representative image of the RNF8 L451D mutation on DNA DSB repair via a RNF8/53BP1 IRIF time course. Wild type RNF8 reconstituted MEFs are in the *left panel,* and L451D RNF8 MEFs are in the *right panel*. RNF8 is *red,* and 53BP1 is *green* in the *merged images*. The tonal range of cell images was rescaled from 0 to 255 in Photoshop to increase the overall contrast for display. *C,* individual assessment of the RNF8 foci per cell of WT and L451D cells. Cells with ≥10 RNF8 foci per cell were examined to ensure only RNF8-positive cells were analyzed, to avoid inclusion of spurious non-IR induced foci, and increased diffuse background stain in later time points. The experiment was done in triplicate, and data were pooled with at least 120 cells per time point and standard error of the mean is included. *, $p < 0.005$ comparing WT and L451D for each time point using a two-tailed Student's *t* test.

signal. We found that the GFP-RNF168-dMIU-BRCT construct rescues 53BP1 recruitment in RNF8$^{-/-}$ MEFs, whereas BRCA1 and FK2 remained unaffected (Fig. 9). This effect is not due to the overexpression of RNF168 as reintroduction of RNF168 lacking the targeting motifs (GFP-RNF168-dMIU) did not restore 53BP1 foci in RNF8$^{-/-}$ MEFs. It should be noted that the GFP-RNF168-dMIU-BRCT chimera forms foci in the absence of permeabilization before fixation, whereas the GFP-RNF168-dMIU chimera does not (data not shown). In addition, the chimeras do not prevent endogenous MDC1 binding at the DSB sites (data not shown). Similar results were obtained when L451D RNF8 MEFs were used instead of RNF8$^{-/-}$ MEFs (Fig. 9). Taken together, these data suggest that not only does RNF8 target RNF168 to DNA damage foci, but moreover that its Lys-63-mediated polyubiquitin chains are required for BRCA1 and FK2 foci formation through stimulation of Ubc13 catalytic activity.

Discussion

The mechanism of activation of E2 enzymes by RING E3 ligases has been enigmatic. Here, combined structural, biochemical, and mutation results further support the hypothesis that RING E3 ligases activate E2 enzymes by imposing conformational selection on the E2~Ub conjugate, so that the ubiquitin molecule occupies a catalytically active conformation more frequently (28, 29, 56). The crystal structure of RNF8-Ubc13~Ub furthermore reveals that the RNF8 dimer can be doubly loaded with an Ubc13~Ub and that both ubiquitin molecules in such a complex can exist in the closed, active conformation. These results and concepts for the RNF8 complex support and broaden the implications from the recent structure of RNF4-Ubc13~Ub/Mms2 (37).

Based upon our RNF8-Ubc13~Ub structure, we hypothesized that two residues, Leu-451 and Arg-441, are critical to stabilize the covalently linked ubiquitin in the closed conformation that is primed for catalysis. The L451D mutation severely impairs RNF8 E2 stimulating activity, consistent with the results from analogous mutations in the RNF4-UbcH5a (Fig. 2) and RING-U-box:UbcH5c systems (29, 51, 56). A superposition of multiple RING E3 ligase dimers/heterodimers onto the RING of RNF8 in the RNF8-Ubc13~Ub structure suggests that both hydrophobic and positively charged basic residues may mediate the E2 stimulation mechanism of these E3s (Fig. 10). BARD1-BRCA1 (57), TRAF6 (58), and CHIP (59, 60) all stimulate E2s to make polyubiquitin chains *in vitro*. These superpositions suggest that TRAF6 may utilize an Arg to stimulate the E2s. There are two negatively charged acidic residues at the end of the ubiquitin α-helix, Asp-32 and Glu-34, which, together with the negative helix dipole, are suitable to provide an electrostatic interaction for a positively charged residue contact in the E3. TRAF6 may additionally engage the ubiquitin with a His on its first zinc finger domain, which makes a close approach to the ubiquitin Asp-32 in our model. Similar to RNF8, it is likely that a Leu in the U-box E3 CHIP mediates ubiquitin contact, although BRCA1 probably engages with a Thr, and possibly a Ser (Fig. 10).

Interestingly, the R441A mutation had little effect on the E3 ligase activity of RNF8, whereas similar mutations in other RING E3s have dramatic effects on catalysis. For example, in the E4B-UbcH5c~Ub system, mutation of the analogous Arg in E4B to Ala (R1143A) reduced the rate of E2~Ub oxyester hydrolysis and auto-ubiquitination (29). Similarly the analogous Arg to Ala mutation in RNF4 was severely impaired in a single-

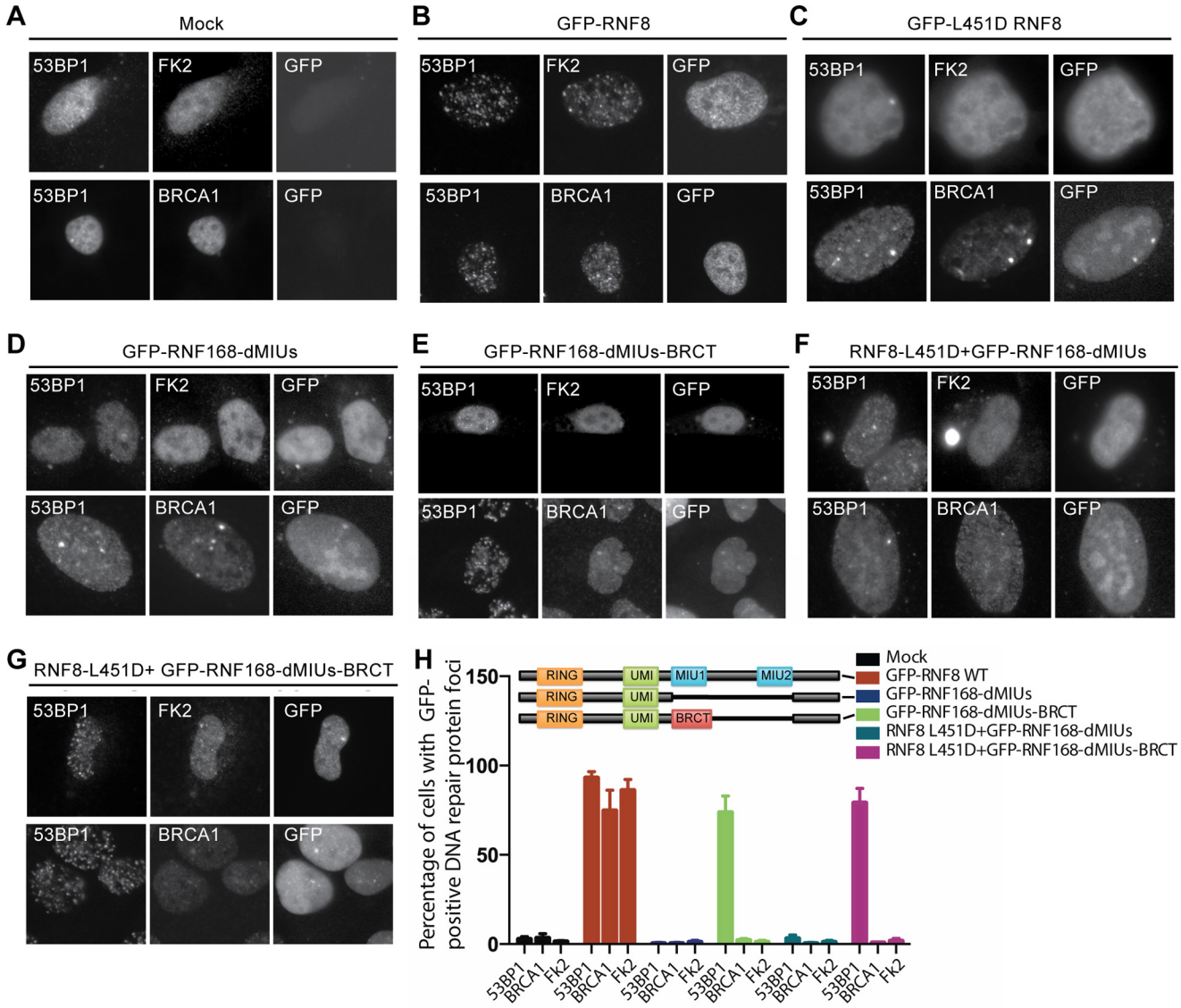

FIGURE 9. **Targeting of RNF168 to sites of DNA DSBs in the absence of its MIUs using a BRCT chimera.** RNF8 knock-out MEFs were transfected with different chimeric constructs as indicated for 24 h. Cells were then irradiated with 2 Gy and left to recover for 30 min at 37 °C. Cells were then fixed and stained as indicated. *A*, mock transfection treatment. *B*, GFP-RNF8 transfection into RNF8$^{-/-}$ MEFs. *C*, GFP-L451D RNF8 transfection into RNF8$^{-/-}$ MEFs. *D*, GFP-RNF168-dMIU transfected into RNF8$^{-/-}$ MEFs. *E*, GFP-RNF168-dMIU-BRCT transfected into RNF8$^{-/-}$ MEFs. *F*, GFP-RNF168-dMIU transfected into RNF8$^{-/-}$ MEFs stably reconstituted with RNF8 L451D. *G*, GFP-RNF168-dMIU-BRCT transfected into RNF8$^{-/-}$ MEFs stably reconstituted with RNF8 L451D. Cells were stained with primary antibodies against 53BP1, BRCA1, and FK2 as detailed under "Experimental Procedures." *H*, quantification of the percentage of cells with GFP-positive DNA repair protein foci. *Error bars* represent standard deviation of three independent experiments with total number of cells equal to 20. GFP-RNF8 constructs in *B* and *C* are not fusion proteins but instead indicate transient coexpression of separate GFP and RNF8 polypeptides from the same expression vector. The GFP stain is therefore not expected to form foci but serves as a transfection control. Schematic of RNF168 chimeras in which the RNF168 MIUs were either removed or replaced with MDC1 BRCT domain are shown *above* graph.

turnover substrate-ubiquitination assay with UbcH5a (51). This difference suggests that the conserved Arg proposed to be a "linchpin" residue in RING E3-mediated E2 stimulation does not play a similar role in RNF8 (29). We suggest that the limited effect of the Arg mutation in RNF8 compared with E4B may reflect the fact that RNF8 forms a stable homodimer, whereas E4B is a monomer in solution (61). The Leu-451 residue in RNF8 resides on the opposite dimer-mediated protomer, which is absent in E4B monomer. An alternative explanation is that the neighboring lysine in RNF8 (Lys-442) could play a role in an allosteric mechanism; however, in the high resolution structure of RNF8 (8), the loop that contains both Lys-442 and Arg-441 is stabilized by the interactions of Cys-437 and Cys-440 in the zinc finger. This suggests a high energy barrier to reorient Lys-442 to face the E2, which would be much less favorable than employing the less restricted Arg-441 for such a mechanism.

The development of an E2 stimulation-deficient RNF8 mutant allowed us to investigate whether the closed ubiquitin conformation is truly related to RNF8 stimulation of Ubc13 catalytic ability. To directly assess the impact of the L451D mutation on the conformation of the covalently tethered ubiquitin, we used small angle x-ray scattering to derive conformational ensembles of RNF8-Ubc13~Ub in solution. Whether generated by the MES or GAJOE genetic algorithms, our ensembles consistently showed 20–30% enhancement of the closed ubiquitin conformation compared with more extended

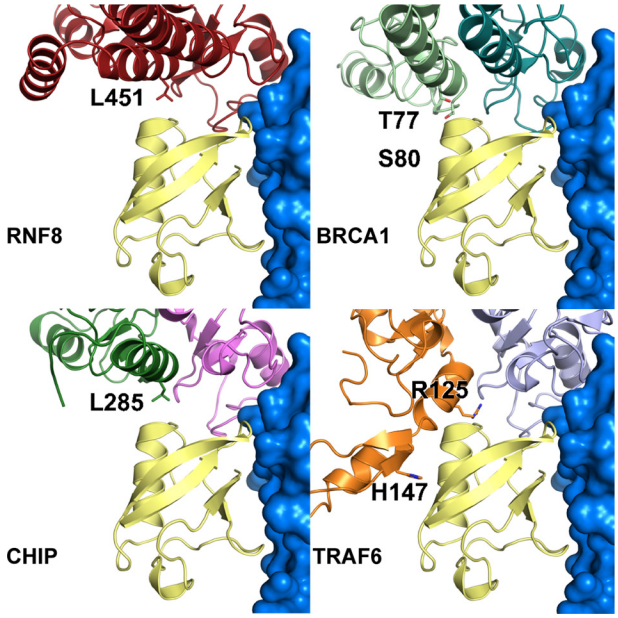

FIGURE 10. **Comparisons of RING E3 dimers and heterodimers relative to E2~Ub.** The E2s of the BARD1-BRCA1 (*teal/green*; PDB code 1JM7), CHIP (*green/violet*; PDB code 2C2V), and TRAF6 (*orange*; PDB code 3HCS) structures were superimposed on the Ubc13 in the RNF8-Ubc13~Ub (*red/blue*) crystal structure. Possible interacting residues are labeled. The TRAF6 structure includes a zinc finger connected to its RING. In all images Ubc13 is *blue* with surface representation, and ubiquitin is *yellow*.

open states in complexes containing WT RNF8 compared with complexes with the L451D mutant (Figs. 4 and 5). The observation that mutants that change conformational sampling without otherwise distorting the fold or assembly can selectively alter biological outcomes was also recently found for the multifunctional DNA double strand break repair ATPase RAD50 (62), suggesting that this strategy of altering the average conformational state offers a promising approach for dissection of function mutations in protein complexes.

A model to reconcile previous evidence that RNF8 is required for downstream RNF168 recruitment (17) has recently been proposed (23). Our results show that RNF8 is indeed required to stimulate Ubc13-dependent Lys-63-ubiquitin chain formation at the sites of DNA DSBs to recruit downstream factors such as BRCA1, for homologous recombination repair to complement and extend the report by Thorslund *et al.* (23). The L451D RNF8 mutant demonstrates that the ability of RNF8 to catalytically enhance Ubc13 is essential for the DNA damage response. Previous studies focused on mutations that either deleted the RING domain or mutated key cysteine residues within the RING. Such mutations demonstrated the necessity of a functional E3 but did not distinguish between the recruitment and catalytic functions of the E3. This is important, as the role of a RING domain could, in some cases, be simply to recruit an E2 enzyme to a site where it is then transferred to another E3 enzyme to form ubiquitin conjugates. Therefore, RNF168 targeted to chromatin cannot functionally replace RNF8 at sites of DNA DSBs in the context of homologous recombination, but it can bypass the role of RNF8 in 53BP1 recruitment for non-homologous end joining.

Here, we show that a single point mutation in RNF8, which specifically abrogates its E2 stimulating activity but not its ability to bind to the sites of DNA damage, blocks DNA damage-associated Lys-63-linked ubiquitination and downstream signaling. We proposed that the necessity for a RING E3's E2 stimulating activity likely extends to other RING E3 ligases (Fig. 10), and this activity is required for their individual roles in the cell. Our combined observation and concept has implications for potential therapeutic strategies. Inhibitors that block protein-protein interactions are notoriously challenging and have met with limited success. Our work presents a novel avenue for blocking RING E3-mediated E2-stimulation, which we show to be critical for the DNA damage response, and likely for many other pathways that involve RING E3s. Such a strategy would take advantage of the extended interface created by the RNF8-Ubc13 complex. Inhibitors that bind this surface could block the ability of the donor ubiquitin to adopt the closed conformation, preventing activation.

Author Contributions—C. D. H. expressed, purified, crystallized proteins, solved structures, performed mutagenesis and *in vitro* ubiquitination assays, and completed cellular assays and data analysis. I. H. I. completed cellular assays, immunoprecipitations, and data analysis. R. A. E. solved structures and performed data analysis. G. L. H. collected SAXS data and contributed to analysis. A. T. X. purified proteins for SAXS. M. J. H. and J. A. T. contributed to data analysis. J. N. M. G. conceived the project and contributed to data and structural analysis. C. D. H. and J. N. M. G. wrote the paper with input from all other authors.

Acknowledgments—We thank S. Classen at the Advanced Light Source (SIBYLS) for crystallographic data collections and support. We also thank the Cellular Imaging Facility at the Cross Cancer Institute for the use of microscopes. We thank X. Yu, Division of Molecular Medicine and Genetics, University of Michigan Medical School, Ann Arbor, MI, for the gift of the RNF8 knock-out MEFs. SAXS data collection and analysis at SIBYLS BL12.3.1 at the Advanced Light Source were supported by the Integrated Diffraction Analysis Technologies Program (Department of Energy/Biological and Environmental Research) and by National Institutes of Health MINOS Grant GM105404.

References

1. Pickart, C. M., and Eddins, M. J. (2004) Ubiquitin: structures, functions, mechanisms. *Biochim. Biophys. Acta* **1695,** 55–72
2. Haas, A. L., and Siepmann, T. J. (1997) Pathways of ubiquitin conjugation. *FASEB J.* **11,** 1257–1268
3. Dye, B. T., and Schulman, B. A. (2007) Structural mechanisms underlying posttranslational modification by ubiquitin-like proteins. *Annu. Rev. Biophys. Biomol. Struct.* **36,** 131–150
4. Komander, D., and Rape, M. (2012) The ubiquitin code. *Annu. Rev. Biochem.* **81,** 203–229
5. Metzger, M. B., Pruneda, J. N., Klevit, R. E., and Weissman, A. M. (2014) RING-type E3 ligases: master manipulators of E2 ubiquitin-conjugating enzymes and ubiquitination. *Biochim. Biophys. Acta* **1843,** 47–60
6. Berndsen, C. E., and Wolberger, C. (2014) New insights into ubiquitin E3 ligase mechanism. *Nat. Struct. Mol. Biol.* **21,** 301–307
7. Campbell, S. J., Edwards, R. A., Leung, C. C., Neculai, D., Hodge, C. D., Dhe-Paganon, S., and Glover, J. N. (2012) Molecular insights into the function of RING finger (RNF)-containing proteins hRNF8 and hRNF168 in Ubc13/Mms2-dependent ubiquitylation. *J. Biol. Chem.* **287,** 23900–23910
8. Mattiroli, F., Vissers, J. H., van Dijk, W. J., Ikpa, P., Citterio, E., Vermeulen, W., Marteijn, J. A., and Sixma, T. K. (2012) RNF168 ubiquitinates K13–15

on H2A/H2AX to drive DNA damage signaling. *Cell* **150,** 1182–1195
9. Plans, V., Scheper, J., Soler, M., Loukili, N., Okano, Y., and Thomson, T. M. (2006) The RING finger protein RNF8 recruits UBC13 for lysine 63-based self-polyubiquitylation. *J. Cell. Biochem.* **97,** 572–582
10. Huen, M. S., Grant, R., Manke, I., Minn, K., Yu, X., Yaffe, M. B., and Chen, J. (2007) RNF8 transduces the DNA-damage signal via histone ubiquitylation and checkpoint protein assembly. *Cell* **131,** 901–914
11. Kolas, N. K., Chapman, J. R., Nakada, S., Ylanko, J., Chahwan, R., Sweeney, F. D., Panier, S., Mendez, M., Wildenhain, J., Thomson, T. M., Pelletier, L., Jackson, S. P., and Durocher, D. (2007) Orchestration of the DNA-damage response by the RNF8 ubiquitin ligase. *Science* **318,** 1637–1640
12. Mailand, N., Bekker-Jensen, S., Faustrup, H., Melander, F., Bartek, J., Lukas, C., and Lukas, J. (2007) RNF8 ubiquitylates histones at DNA double strand breaks and promotes assembly of repair proteins. *Cell* **131,** 887–900
13. Wang, B., and Elledge, S. J. (2007) Ubc13/Rnf8 ubiquitin ligases control foci formation of the Rap80/Abraxas/Brca1/Brcc36 complex in response to DNA damage. *Proc. Natl. Acad. Sci. U.S.A.* **104,** 20759–20763
14. Wang, B., Matsuoka, S., Ballif, B. A., Zhang, D., Smogorzewska, A., Gygi, S. P., and Elledge, S. J. (2007) Abraxas and RAP80 form a BRCA1 protein complex required for the DNA damage response. *Science* **316,** 1194–1198
15. Sato, Y., Yoshikawa, A., Mimura, H., Yamashita, M., Yamagata, A., and Fukai, S. (2009) Structural basis for specific recognition of Lys 63-linked polyubiquitin chains by tandem UIMs of RAP80. *EMBO J.* **28,** 2461–2468
16. Penengo, L., Mapelli, M., Murachelli, A. G., Confalonieri, S., Magri, L., Musacchio, A., Di Fiore, P. P., Polo, S., and Schneider, T. R. (2006) Crystal structure of the ubiquitin binding domains of rabex-5 reveals two modes of interaction with ubiquitin. *Cell* **124,** 1183–1195
17. Doil, C., Mailand, N., Bekker-Jensen, S., Menard, P., Larsen, D. H., Pepperkok, R., Ellenberg, J., Panier, S., Durocher, D., Bartek, J., Lukas, J., and Lukas, C. (2009) RNF168 binds and amplifies ubiquitin conjugates on damaged chromosomes to allow accumulation of repair proteins. *Cell* **136,** 435–446
18. Polo, S. E., and Jackson, S. P. (2011) Dynamics of DNA damage response proteins at DNA breaks: a focus on protein modifications. *Genes Dev.* **25,** 409–433
19. Williams, R. S., Williams, J. S., and Tainer, J. A. (2007) Mre11-Rad50-Nbs1 is a keystone complex connecting DNA repair machinery, double strand break signaling, and the chromatin template. *Biochem. Cell Biol.* **85,** 509–520
20. Spycher, C., Miller, E. S., Townsend, K., Pavic, L., Morrice, N. A., Janscak, P., Stewart, G. S., and Stucki, M. (2008) Constitutive phosphorylation of MDC1 physically links the MRE11-RAD50-NBS1 complex to damaged chromatin. *J. Cell Biol.* **181,** 227–240
21. Stucki, M., Clapperton, J. A., Mohammad, D., Yaffe, M. B., Smerdon, S. J., and Jackson, S. P. (2005) MDC1 directly binds phosphorylated histone H2AX to regulate cellular responses to DNA double strand breaks. *Cell* **123,** 1213–1226
22. Lee, M. S., Edwards, R. A., Thede, G. L., and Glover, J. N. (2005) Structure of the BRCT repeat domain of MDC1 and its specificity for the free COOH-terminal end of the γ-H2AX histone tail. *J. Biol. Chem.* **280,** 32053–32056
23. Thorslund, T., Ripplinger, A., Hoffmann, S., Wild, T., Uckelmann, M., Villumsen, B., Narita, T., Sixma, T. K., Choudhary, C., Bekker-Jensen, S., and Mailand, N. (2015) Histone H1 couples initiation and amplification of ubiquitin signalling after DNA damage. *Nature* **527,** 389–393
24. Stewart, G. S., Panier, S., Townsend, K., Al-Hakim, A. K., Kolas, N. K., Miller, E. S., Nakada, S., Ylanko, J., Olivarius, S., Mendez, M., Oldreive, C., Wildenhain, J., Tagliaferro, A., Pelletier, L., Taubenheim, N., *et al.* (2009) The RIDDLE syndrome protein mediates a ubiquitin-dependent signaling cascade at sites of DNA damage. *Cell* **136,** 420–434
25. Ciccia, A., and Elledge, S. J. (2010) The DNA damage response: making it safe to play with knives. *Mol. Cell* **40,** 179–204
26. Xie, A., Hartlerode, A., Stucki, M., Odate, S., Puget, N., Kwok, A., Nagaraju, G., Yan, C., Alt, F. W., Chen, J., Jackson, S. P., and Scully, R. (2007) Distinct roles of chromatin-associated proteins MDC1 and 53BP1 in mammalian double strand break repair. *Mol. Cell* **28,** 1045–1057
27. Shibata, A., Moiani, D., Arvai, A. S., Perry, J., Harding, S. M., Genois, M. M., Maity, R., van Rossum-Fikkert, S., Kertokalio, A., Romoli, F., Ismail, A., Ismalaj, E., Petricci, E., Neale, M. J., Bristow, *et al.* (2014) DNA double strand break repair pathway choice is directed by distinct MRE11 nuclease activities. *Mol. Cell* **53,** 7–18
28. Plechanovová, A., Jaffray, E. G., Tatham, M. H., Naismith, J. H., and Hay, R. T. (2012) Structure of a RING E3 ligase and ubiquitin-loaded E2 primed for catalysis. *Nature* **489,** 115–120
29. Pruneda, J. N., Littlefield, P. J., Soss, S. E., Nordquist, K. A., Chazin, W. J., Brzovic, P. S., and Klevit, R. E. (2012) Structure of an E3:E2~Ub complex reveals an allosteric mechanism shared among RING/U-box ligases. *Mol. Cell* **47,** 933–942
30. Dou, H., Buetow, L., Sibbet, G. J., Cameron, K., and Huang, D. T. (2012) BIRC7-E2 ubiquitin conjugate structure reveals the mechanism of ubiquitin transfer by a RING dimer. *Nat. Struct. Mol. Biol.* **19,** 876–883
31. Moraes, T. F., Edwards, R. A., McKenna, S., Pastushok, L., Xiao, W., Glover, J. N., and Ellison, M. J. (2001) Crystal structure of the human ubiquitin conjugating enzyme complex, hMms2-hUbc13. *Nat. Struct. Biol.* **8,** 669–673
32. Carvalho, A. F., Pinto, M. P., Grou, C. P., Vitorino, R., Domingues, P., Yamao, F., Sá-Miranda, C., and Azevedo, J. E. (2012) High-yield expression in *Escherichia coli* and purification of mouse ubiquitin-activating enzyme E1. *Mol. Biotechnol.* **51,** 254–261
33. Classen, S., Hura, G. L., Holton, J. M., Rambo, R. P., Rodic, I., McGuire, P. J., Dyer, K., Hammel, M., Meigs, G., Frankel, K. A., and Tainer, J. A. (2013) Implementation and performance of SIBYLS: a dual end station small-angle x-ray scattering and macromolecular crystallography beamline at the Advanced Light Source. *J. Appl. Crystallogr.* **46,** 1–13
34. Adams, P. D., Afonine, P. V., Bunkóczi, G., Chen, V. B., Davis, I. W., Echols, N., Headd, J. J., Hung, L. W., Kapral, G. J., Grosse-Kunstleve, R. W., McCoy, A. J., Moriarty, N. W., Oeffner, R., Read, R. J., Richardson, D. C., *et al.* (2010) PHENIX: a comprehensive Python-based system for macromolecular structure solution. *Acta Crystallogr. D Biol. Crystallogr.* **66,** 213–221
35. McCoy, A. J. (2007) Solving structures of protein complexes by molecular replacement with Phaser. *Acta Crystallogr. D Biol. Crystallogr.* **63,** 32–41
36. McCoy, A. J., Grosse-Kunstleve, R. W., Adams, P. D., Winn, M. D., Storoni, L. C., and Read, R. J. (2007) Phaser crystallographic software. *J. Appl. Crystallogr.* **40,** 658–674
37. Branigan, E., Plechanovová, A., Jaffray, E. G., Naismith, J. H., and Hay, R. T. (2015) Structural basis for the RING-catalyzed synthesis of Lys-63-linked ubiquitin chains. *Nat. Struct. Mol. Biol.* **22,** 597–602
38. Hura, G. L., Menon, A. L., Hammel, M., Rambo, R. P., Poole, F. L., 2nd, Tsutakawa, S. E., Jenney, F. E., Jr., Classen, S., Frankel, K. A., Hopkins, R. C., Yang, S. J., Scott, J. W., Dillard, B. D., Adams, M. W., and Tainer, J. A. (2009) Robust, high-throughput solution structural analyses by small angle x-ray scattering (SAXS). *Nat. Methods* **6,** 606–612
39. Dyer, K. N., Hammel, M., Rambo, R. P., Tsutakawa, S. E., Rodic, I., Classen, S., Tainer, J. A., and Hura, G. L. (2014) High-throughput SAXS for the characterization of biomolecules in solution: a practical approach. *Methods Mol. Biol.* **1091,** 245–258
40. Konarev, P. V., Volkov, V. V., Sokolova, A. V., Koch, M. H. J., and Svergun, D. I. (2003) PRIMUS: a Windows PC-based system for small-angle scattering data analysis. *J. Appl. Crystallogr.* **36,** 1277–1282
41. Putnam, C. D., Hammel, M., Hura, G. L., and Tainer, J. A. (2007) X-ray solution scattering (SAXS) combined with crystallography and computation: defining accurate macromolecular structures, conformations and assemblies in solution. *Q. Rev. Biophys.* **40,** 191–285
42. Svergun, D. I. (1992) Determination of the regularization parameter in indirect-transform methods using perceptual criteria. *Acta Crystallogr.* **25,** 495–503
43. Pelikan, M., Hura, G., and Hammel, M. (2009) Structure and flexibility within proteins as identified through small angle x-ray scattering. *Gen. Physiol. Biophys.* **28,** 174–189
44. Schneidman-Duhovny, D., Hammel, M., and Sali, A. (2010) FoXS: a web server for rapid computation and fitting of SAXS profiles. *Nucleic Acids Res.* **38,** W540–W544
45. Schneidman-Duhovny, D., Hammel, M., Tainer, J. A., and Sali, A. (2013) Accurate SAXS profile computation and its assessment by contrast variation experiments. *Biophys. J.* **105,** 962–974

46. Tria, G., Mertens, H. D., Kachala, M., and Svergun, D. I. (2015) Advanced ensemble modelling of flexible macromolecules using x-ray solution scattering. *IUCrJ* **2,** 207–217
47. Hodge, C. D., Edwards, R. A., Markin, C. J., McDonald, D., Pulvino, M., Huen, M. S., Zhao, J., Spyracopoulos, L., Hendzel, M. J., and Glover, J. N. (2015) Covalent inhibition of Ubc13 affects ubiquitin signaling and reveals active site elements important for targeting. *ACS Chem. Biol.* **10,** 1718–1728
48. Minter-Dykhouse, K., Ward, I., Huen, M. S., Chen, J., and Lou, Z. (2008) Distinct *versus* overlapping functions of MDC1 and 53BP1 in DNA damage response and tumorigenesis. *J. Cell Biol.* **181,** 727–735
49. Carpenter, A. E., Jones, T. R., Lamprecht, M. R., Clarke, C., Kang, I. H., Friman, O., Guertin, D. A., Chang, J. H., Lindquist, R. A., Moffat, J., Golland, P., and Sabatini, D. M. (2006) CellProfiler: image analysis software for identifying and quantifying cell phenotypes. *Genome Biol.* **7,** R100
50. Kamentsky, L., Jones, T. R., Fraser, A., Bray, M. A., Logan, D. J., Madden, K. L., Ljosa, V., Rueden, C., Eliceiri, K. W., and Carpenter, A. E. (2011) Improved structure, function and compatibility for CellProfiler: modular high-throughput image analysis software. *Bioinformatics* **27,** 1179–1180
51. Plechanovová, A., Jaffray, E. G., McMahon, S. A., Johnson, K. A., Navrátilová, I., Naismith, J. H., and Hay, R. T. (2011) Mechanism of ubiquitylation by dimeric RING ligase RNF4. *Nat. Struct. Mol. Biol.* **18,** 1052–1059
52. Hurley, J. H., Lee, S., and Prag, G. (2006) Ubiquitin-binding domains. *Biochem. J.* **399,** 361–372
53. Das, R., Liang, Y. H., Mariano, J., Li, J., Huang, T., King, A., Tarasov, S. G., Weissman, A. M., Ji, X., and Byrd, R. A. (2013) Allosteric regulation of E2:E3 interactions promote a processive ubiquitination machine. *EMBO J.* **32,** 2504–2516
54. Rambo, R. P., and Tainer, J. A. (2011) Characterizing flexible and intrinsically unstructured biological macromolecules by SAS using the Porod-Debye law. *Biopolymers* **95,** 559–571
55. Huen, M. S., Huang, J., Yuan, J., Yamamoto, M., Akira, S., Ashley, C., Xiao, W., and Chen, J. (2008) Noncanonical E2 variant-independent function of UBC13 in promoting checkpoint protein assembly. *Mol. Cell. Biol.* **28,** 6104–6112
56. Soss, S. E., Klevit, R. E., and Chazin, W. J. (2013) Activation of UbcH5c∼Ub is the result of a shift in interdomain motions of the conjugate bound to U-box E3 ligase E4B. *Biochemistry* **52,** 2991–2999
57. Hashizume, R., Fukuda, M., Maeda, I., Nishikawa, H., Oyake, D., Yabuki, Y., Ogata, H., and Ohta, T. (2001) The RING heterodimer BRCA1-BARD1 is a ubiquitin ligase inactivated by a breast cancer-derived mutation. *J. Biol. Chem.* **276,** 14537–14540
58. Yin, Q., Lin, S. C., Lamothe, B., Lu, M., Lo, Y. C., Hura, G., Zheng, L., Rich, R. L., Campos, A. D., Myszka, D. G., Lenardo, M. J., Darnay, B. G., and Wu, H. (2009) E2 interaction and dimerization in the crystal structure of TRAF6. *Nat. Struct. Mol. Biol.* **16,** 658–666
59. Zhang, M., Windheim, M., Roe, S. M., Peggie, M., Cohen, P., Prodromou, C., and Pearl, L. H. (2005) Chaperoned ubiquitylation–crystal structures of the CHIP U box E3 ubiquitin ligase and a CHIP-Ubc13-Uev1a complex. *Mol. Cell* **20,** 525–538
60. Soss, S. E., Yue, Y., Dhe-Paganon, S., and Chazin, W. J. (2011) E2 conjugating enzyme selectivity and requirements for function of the E3 ubiquitin ligase CHIP. *J. Biol. Chem.* **286,** 21277–21286
61. Nordquist, K. A., Dimitrova, Y. N., Brzovic, P. S., Ridenour, W. B., Munro, K. A., Soss, S. E., Caprioli, R. M., Klevit, R. E., and Chazin, W. J. (2010) Structural and functional characterization of the monomeric U-box domain from E4B. *Biochemistry* **49,** 347–355
62. Deshpande, R. A., Williams, G. J., Limbo, O., Williams, R. S., Kuhnlein, J., Lee, J. H., Classen, S., Guenther, G., Russell, P., Tainer, J. A., and Paull, T. T. (2014) ATP-driven Rad50 conformations regulate DNA tethering, end resection, and ATM checkpoint signaling. *EMBO J.* **33,** 482–500
63. Pollard, T. D. (2010) A guide to simple and informative binding assays. *Mol. Biol. Cell* **21,** 4061–4067
64. Saito, T., Nakamura, A., Aoki, Y., Yokoto, T., Okada, T., Osawa, M., and Takeda, S. (2010) Antisense PMO found in dystrophic dog model was effective in cells from exon 7-deleted DMD patient. *PLoS One* **5,** e12239